Journal of Human Evolution 182 (2023) 103401

Contents lists available at ScienceDirect

Journal of Human Evolution

journal homepage: www.elsevier.com/locate/jhevol

Functional morphological integration related to feeding biomechanics in the hominine skull

Hyunwoo Jung [a, *], David Strait [b, c], Campbell Rolian [d], Karen L. Baab [a]

[a] Department of Anatomy, College of Graduate Studies, Midwestern University, Glendale, AZ 85308, USA
[b] Department of Anthropology, Washington University in St. Louis, St. Louis, MO 63130, USA
[c] Palaeo-Research Institute, University of Johannesburg, Auckland Park, Johannesburg 2092, South Africa
[d] Department of Anatomy and Cell Biology, McGill University, Montreal, QC H3A 0C7, Canada

ARTICLE INFO

Article history:
Received 21 November 2022
Accepted 21 May 2023
Available online 28 August 2023

Keywords:
Morphological covariation
Evolvability statistics
Morphological evolution
Evolution of cranio-mandibular architecture
Quantitative genetics

ABSTRACT

Quantifying and characterizing the pattern of trait covariances is crucial for understanding how population-level patterns of integration might constrain or facilitate craniofacial evolution related to the feeding system. This study addresses an important gap in our knowledge by investigating magnitudes and patterns of morphological integration of biomechanically informative traits in the skulls of *Homo sapiens*, *Pan troglodytes*, and *Gorilla gorilla*. We predicted a lower magnitude of integration among human biomechanical traits since humans eat a softer, less biomechanically challenging diet than apes. Indeed, compared to African apes, the magnitudes of integration were lower in *H. sapiens* skulls for form data (raw dimensions) but were similar or higher for shape data (raw dimensions scaled by geometric mean). Patterns of morphological integration were generally similar, but not identical, across the three species, particularly for the form data compared to the shape data. Traits that load heavily on the primary axis of variation in morphospace are generally associated with size and/or shape of the temporalis and masseter muscles and with dimensions related to the constrained lever model of jaw biomechanics. Given the conserved nature of morphological integration, skull adaptations for food processing in African apes and humans may have been constrained to occur along certain paths of high evolvability. The conserved pattern of functional integration also indicates that extant hominine species can operate as reasonable analogues for extinct hominins in studies that require population-level patterns of trait variance/covariance.

1. Introduction

Musculoskeletal and dental traits must function jointly to effectively process food and should thus covary in size and shape as a functional unit, that is, the traits should be integrated (e.g., Olson and Miller, 1958; Cheverud 1996; Gómez-Robles and Polly, 2012; Noback and Harvati, 2015). Functional integration can arise from mechanical, developmental, epigenetic, and/or genetic factors (Klingenberg, 2014). Indeed, the idea that biomechanically important traits of the primate skull are integrated is pervasive. Biomechanical traits of the skull are often grouped into functional complexes (modules) when analyzing phylogenetic relationships to avoid overweighting what is essentially a single complex trait (Skelton and McHenry, 1992; Strait, 2001; Lockwood, 2007). A module refers to a structure that shows stronger within-structure trait interactions than between-structure trait interactions (Olson and Miller, 1958; Cheverud, 1996; Klingenberg, 2014). The common view that the feeding system in primates and other mammals reflects functional trade-offs between feeding biomechanics and other skull functions (e.g., social signaling via gape, protection and support of sense organs) is also consistent with an integrated system (Herring and Herring, 1974; Ravosa, 1998; Dumont and Herrel, 2003; Ross and Iriarte-Diaz, 2019). Polly (2020) suggests that functional trade-offs may produce intermediate morphologies that, while suboptimal for either function, are nevertheless the optimal solution in an adaptive landscape with conflicting selective pressures, helping to bridge valleys in the adaptive landscape. Likewise, integration may be beneficial in producing functional equivalence across a range of morphologies (Young et al., 2010). For example, the upper and lower jaws and occlusal surfaces of opposing teeth

* Corresponding author.
E-mail address: hjung@midwestern.edu (H. Jung).

https://doi.org/10.1016/j.jhevol.2023.103401
0047-2484/

must conform to break down food (e.g., Gómez-Robles and Polly, 2012) and bony architecture must resist the strains produced by the chewing muscles (e.g., Hylander, 1988; Hylander et al., 1998; Vinyard et al., 2011).

Functional integration is also implicit in some theoretical models of biomechanics. For example, the constrained lever model of jaw biomechanics relates temporomandibular morphology to a need to protect against distraction (i.e., dislocation) during mastication (Greaves, 1978; Spencer, 1999; Fig. 1). A key prediction of the constrained lever model is that balancing side muscle forces may be reduced during molar bites in order to shift the muscle resultant toward the working side and ensure that it remains within the triangle of support. It follows logically from this model that jaw proportions concerning the anteroposterior positioning of the tooth row relative to the temporomandibular joint (TMJ), the breadth between the TMJs, the breadth between the toothrows, and the height of the TMJs above the occlusal plane would be tightly integrated so as to avoid the independent evolution of jaw dimensions that would promote joint distraction. The underlying architecture of the cranium also determines the mechanical advantage of jaw adductors which in turn affects bite force and, ultimately, what food items can be exploited (e.g., Strait et al., 2013). The current study is an important step toward testing these assumptions about functional integration using empirical data related to chewing biomechanics in primates.

1.1. Cranial morphological integration in hominoids

Quantifying and characterizing the pattern of trait covariance is crucial for understanding how population-level patterns of integration might constrain or facilitate craniofacial evolution related to food processing in hominoids, including extinct hominins (i.e., bridging microevolutionary and macroevolutionary processes). Previous evolutionary quantitative genetics analyses have supported a larger role for stochastic processes and a smaller role for directional selection in skull evolution within hominins based on population patterns of trait variance/covariance (Ackermann and Cheverud, 2004; Schroeder et al., 2014; Baab, 2018) and a greater role for stabilizing selection in extant hominoid skull evolution (Schroeder and von Cramon-Taubadel, 2017). Furthermore, there is broad agreement that the pattern of cranial integration is remarkably conserved across hominoids, catarrhines, and even mammals more broadly, but the magnitude of integration is more labile (Cheverud, 1982; Ackermann, 2002; Bastir et al., 2005; Mitteroecker and Bookstein, 2008; de Oliveira et al., 2009; Porto et al., 2009; Goswami and Polly, 2010; Singh et al., 2012; Profico et al., 2017; Neaux, 2017; Neaux et al., 2018). However, these insights are based on generic, rather than explicitly biomechanical, measures of shape.

It is unclear whether, and how, this generally conserved pattern of skull integration applies to traits that influence feeding biomechanics specifically. One possibility is that variation among species in cranial integration is driven by differences in the biomechanical function of the feeding apparatus. Indeed, there is some support for stronger functional integration in capuchins eating mechanically resistant foods (compared to species not eating such foods) based on three-dimensional (3D) landmarks in regions of high strain on the craniofacial skeleton (Makedonska et al., 2012) and stronger integration between the upper dental arch and the attachment shape of jaw adductors in human populations whose diets involve higher strains (Noback and Harvati, 2015). Yet, not all analyses support a link between stronger overall skull integration and mechanically resistant diets. Paschetta et al. (2016) examined modern human groups consuming hard and soft diets using a set of standard cranial osteometric landmarks and semilandmarks representing the temporalis origin. While there are differences in integration magnitude among groups, those consuming higher strain diets are not consistently characterized by higher integration across all regions of the cranium. The limited understanding of how biomechanically relevant skull traits covary within populations is surprising, given the central role attributed to diet and food processing in shaping craniofacial diversity and lineage divergence in primates generally and hominines specifically. The current investigation complements and extends previous analyses of cranial and mandibular integration by focusing on traits that can be tied directly to feeding biomechanics, rather than evaluations of overall cranial shape.

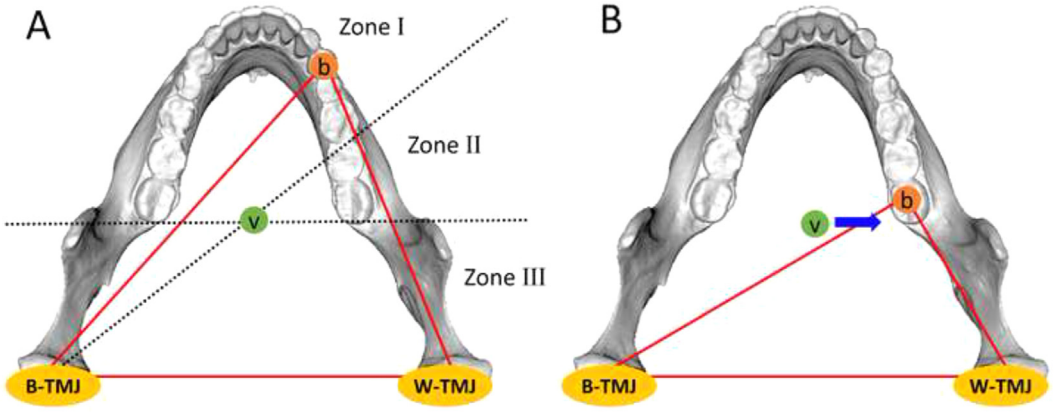

Figure 1. The constrained lever model of jaw biomechanics in human example. A: bite point on P_3; B: bite point on M_3. The jaw apparatus functions as a three-legged stool with bite point (b) and the temporomandibular joints (TMJs) on the working side (W-TMJ) and balancing (i.e., nonbiting) side (B-TMJ). When sitting on such a stool, it is essential that one's center of mass is positioned between the three legs or else the stool will tip over. Similarly, in jaw biomechanics, the vector resultant of the masticatory muscles (v) must be positioned within a 'triangle of support' defined by the bite point and the two TMJs. If the resultant (v) is found outside of the triangle as in B, then the mandible will 'tip over' around an axis defined by the bite point and the balancing side TMJ. This will have the effect of distracting the working (i.e., biting) side TMJ because the condyle will be 'pulled' inferiorly out of the joint. Zones I and II are separated by an oblique line passing through the balancing side TMJ and the vector resultant of the masticatory muscles (v) in the midline, and Zones II and III are separated by a transverse line passing through the vector resultant of the masticatory muscles (v). Thus, if the bite point is in Zone II, the vector resultant of the masticatory muscles (v) must move to inside of the triangle of support by lessening the recruitment of the balancing side masticatory muscles as depicted with the blue arrow in B. TMJ distraction occurs in Zone III as the bite point is posterior to the vector resultant of the masticatory muscles (v). (For interpretation of the references to color in this figure legend, the reader is referred to the web version of this article.)

1.2. Aims and evolutionary implications

The aim of this study is to assess and compare patterns of trait variance and covariance within the cranium and mandible of *Homo sapiens*, *Gorilla gorilla*, and *Pan troglodytes*, which represent species in the three extant genera most closely related to the extinct hominins. We present complementary, evolutionary quantitative genetics tests to compare the magnitudes and pattern of morphological integration and its evolutionary consequences. Three hypotheses were evaluated as follows.

Hypothesis 1. All three species show similar patterns of integration for craniofacial measurements associated with feeding biomechanics. This would be consistent with previous studies that reported similar patterns of integration in the primate cranium, including hominoids, based on general form/shape variables (e.g., de Oliveira et al., 2009; Porto et al., 2009).

Hypothesis 2. *Homo sapiens* will show a distinct pattern of integration relative to the African apes as the skull and feeding apparatus are distinct in humans, including the presence of a globular neurocranium, small orthognathic face, and relatively gracile feeding system (Lieberman, 2011). Patterns of morphological integration may have evolved to allow this fundamental reorganization of the skull in recent humans that in turn affects the pattern of covariance between functionally relevant traits.

Hypothesis 3. African apes have a higher magnitude of integration for biomechanically informative craniofacial measurements than *H. sapiens* who consume a softer, more processed (e.g., agricultural) diet (see also Makedonska et al., 2012; Noback and Harvati, 2015).

2. Materials and methods

2.1. Skeletal samples

We used 119 crania and 98 mandibles of *H. sapiens*, 81 crania and 79 mandibles of *Pan troglodytes troglodytes/Pan troglodytes schweinfurthii*, and 101 crania and 92 mandibles of *G. gorilla* to compare the patterns of variance and covariance among biomechanically informative traits of the skull (Table 1). The crania and mandibles were scanned using a Creaform ExaScan 3D laser scanner (Creaform, Québec), a Breuckmann optical white light scanner (Breuckmann GmbH, Braunschweig/Meersburg), an HDI-120 structured-light scanner (LMI technologies INC., Vancouver), and an Artec Space Spider scanner (Artec 3D, Senningerberg). All individuals were adults as judged by a (fully) fused spheno-occipital synchondrosis and/or on the third molars being in full occlusion. Specimens with obvious pathologies and those missing more than six landmarks in the cranium or mandible were excluded from this study. It was our observation that most missing landmarks were due to absent teeth or damage to the alveolar region. An arbitrary threshold of six landmarks was used to exclude those specimens missing a large number of landmarks from a limited anatomical region as missing data imputation in this circumstance is ill-advised. The maximum number of missing landmarks was 5 in the cranium and 3 in the mandible. The sampling strategy was twofold: maximizing sample sizes while minimizing between-population variation. Since variance/covariance matrices are intended to capture population parameters, we aimed to restrict population/geographic variation while sampling $n \sim 100$ per species. The sampling strategy was applied consistently to all taxa but nevertheless has slightly different outcomes based on data availability. Specifically, we were able to measure variation properties from a single *H. sapiens* sample, a single *Gorilla* subspecies (*Gorilla gorilla gorilla*), and two closely related *Pan* populations/subspecies. *Homo sapiens* specimens are from an archaeological cemetery from a Meroitic period (ca. 350 BC to AD 350) Nubian site of Semna, South on the Upper Nile River, Sudan, that are housed in the School of Human Evolution and Social Change at Arizona State University. This period of Nubian occupation of the Nile River is characterized by agriculture and animal husbandry (Hakem, 1981; Galland et al., 2016). *Pan troglodytes* specimens were sampled from two closely related subspecies *P. t. troglodytes* and *P. t. schweinfurthii* (Prado-Martinez et al., 2013) who experienced recent, substantial gene flow and may be better viewed as populations (Lester et al., 2021). The majority of *P. t. troglodytes* and *P. t. schweinfurthii* were from the Cleveland Museum of Natural History (Cleveland, USA) and the Royal Museum for Central Africa (Tervuren, Belgium), respectively, with smaller numbers from the American Museum of Natural History (New York City, USA), the Field Museum of Natural History (Chicago, USA), the Museum of Comparative Zoology (Cambridge, USA), and the Smithsonian Museum of Natural History (Washington D.C., USA). *Gorilla gorilla gorilla* specimens are housed in the Cleveland Museum of Natural History (Cleveland, USA). Some 3D surface scans of the recent humans were provided by Claire Terhune (University of Arkansas), whereas those of most chimpanzees and gorillas were provided by Jason Massey (Monash University) and Kieran McNulty (University of Minnesota). The remaining specimens were scanned by H.J. for the current study.

2.2. Landmarks and interlandmark distances

The raw data for this study comprised 29 linear dimensions of the cranium and 20 linear dimensions of the mandible that capture variation related to bite force (size and mechanical advantage of muscles of mastication; load arms at bite points), joint loading at the TMJ, bone strength (ability to resist strain), the 'triangle of support' of the constrained lever model of jaw biomechanics (Greaves, 1978; Spencer, 1999; Fig. 1), tooth crown strength, and dental occlusal area and gape (Table 2; Fig. 2). These linear dimensions were calculated as interlandmark distances from 3D landmarks using the 'interlmkdist' function in the 'geomorph' package v. 4.0.3. (Baken et al., 2021) in R v. 4.1.1. (R Core Team, 2021). The 3D landmarks were recorded from the left side of the cranium and mandible (right side if the left side was damaged) or bilaterally when the associated measurement crossed the midline (Supplementary Online Material [SOM] Table S1; Fig. 2), using the 3D Slicer v. 4.11.20210226 software (Fedorov et al., 2012). There are two main reasons for using interlandmark distances rather than

Table 1
Sample description.

Genus	(Sub)species	Cranium	Mandible
Homo	*sapiens*	119 (F = 52; M = 67)	98 (F = 37; M = 61)
Pan	*troglodytes troglodytes*	62 (F = 36; M = 26)	58 (F = 34; M = 24)
Pan	*troglodytes schweinfurthii*	19 (F = 5; M = 14)	21 (F = 4; M = 17)
Gorilla	*gorilla gorilla*	101 (F = 53; M = 48)	92 (F = 44; M = 48)

Abbreviation: F = female; M = male.

Table 2
Biomechanical measurements based on interlandmark distances.

Measurement		Definition	Mechanical significance	Landmarks in SOM Table S1
Cranium				
1	Breadth of midzygomatic arch (Br_midzygo)	Midzygomatic arch outer to midzygomtic arch inner	Bending strength in transverse plane (i.e., resisting action of deep masseter)	ZAO:ZAI
2	Height of midzygomatic arch (Ht_midzygo)	Midzygomatic arch superior to midzygomatic arch inferior as measured between the superiormost and inferiormost points on the zygomatic arch in the same coronal plane as midzygomatic arch outer	Bending strength in sagittal plane (i.e., resisting action of superior and deep masseter)	ZAS:ZAI
3	Maximum length of temporal foramen (MaxLn_tempfora)	Posteriormost point on the anterior margin of the supraglenoid gutter (posterior temporal foramen) to the anteriormost point of the temporal foramen on the zygomatic bone (anterior temporal foramen) in the same plane as ZAO and ZAI	Related to temporal foramen size; roughly proportional to temporalis cross sectional area, should be correlated with maximum force of temporalis	PTF:ATF
4	Maximum breadth of the temporal foramen (MaxBr_tempfora)	Maximum breadth of the temporal foramen from the inner surface of the zygomatic arch (lateral temporal foramen) to the neurocranial wall in the same coronal plane (medial temporal foramen)	Related to temporal foramen size; roughly proportional to temporalis cross sectional area, should be correlated with maximum force of temporalis	LTF:MTF
5	Bi-zygomatic breadth (Bi_zygo)	Right to left midzygomatic arch outer	Related to size of the temporalis and orientation of deep masseter	ZAO_left:ZAO_right
6	Maximum length of the temporalis origin (Temp_Ln)	Posteriormost point on temporalis origin (posterior temporalis) to anteriormost point on temporalis origin (anterior temporalis)	Related to shape of the temporalis origin; approximates relative sizes of anterior vs. posterior portions of temporalis muscle	PT:AT
7	Perpendicular height of the temporalis origin (Temp_Ht)	Maximum height of the temporalis origin perpendicular to its chord of maximum length, from the superior temporal line (superior temporalis) to the zygomatic arch (inferior temporalis)	Related to shape of the temporalis origin; approximates relative sizes of anterior vs. posterior portions of temporalis muscle	ST:IT
8	Articular eminence to masseteric tubercle (AE_MT)	Apex of midarticular eminence to masseteric tubercle	Roughly proportional to superficial masseter lever arm, as well as orientation of superficial masseter (as length increases proportionally, superficial masseter may become more inclined); inversely proportional to gape	AE:MT
9	Zygomaticoalveolar expansion (Zygomatico_exp)	Distance from orbitale to midzygomaticoalveolar crest in frontal view	Resistance to shear in coronal plane due to contraction of masseter	O:ZAC
10	Frontomalaretemporale to vertex zygomatic angle (FMT_J)	Frontomalaretemporale to jugale	Related to zygomatic angle; resistance to bending stress due to contraction of masseter	FMT:J
11	Vertex zygomatic angle to superior point of midzygomatic arch (J_ZAS)	Jugale to midzygomatic arch superior	Related to zygomatic angle; resistance to bending stress due to contraction of masseter	J:ZAS
12	Frontomalaretemporale to superior point of midzygomatic arch (FMT_ZAS)	Frontomalaretemporale to midzygomatic arch superior	Related to zygomatic angle; resistance to bending stress due to contraction of masseter	FMT:ZAS
13	Inferolateral breadth of postorbital bar (PO_Br)	From jugale to inferolateral 'corner' of orbit	Related to zygomatic angle; resistance to bending stress due to contraction of masseter	Z:IO
14	Minimum thickness of zygomatic root (AZM_PR)	Minimum distance between a point on 'cheek' in midline plane through anterior temporal foramen at maximal thickness perpendicular to long axis of section and a point on the posterior surface of the root of the zygomatic arch in same horizontal plane as Frankfort Horizontal	Resistance to bending in transverse plane as superficial masseter contracts	AZM:PR
15	Maximum P^4 breadth (P4_Br)			BMP4: LMP4

Table 2 (*continued*)

Measurement		Definition	Mechanical significance	Landmarks in SOM Table S1
		Maximum buccolingual chord distance between buccalmost and lingualmost points on P^4 crown	Related to tooth crown strength (resistance to ribbon fractures), rate of wear, and occlusal area	
16	Maximum M^2 breadth (M2_Br)	Maximum buccolingual chord distance between buccalmost and lingualmost points on M^2 crown	Related to tooth crown strength (resistance to ribbon fractures), rate of wear, and occlusal area	BMM2:LMM2
17	Maxillary premolar alveolar length (P4_alveolar_Ln)	C^1/P^3 buccal alveolar crest to P^4/M^1 buccal alveolar crest	Surrogate for mesiodistal length of premolar crowns, related to tooth crown strength (resistance to ribbon fractures), rate of wear, and occlusal area	C-P3:P4-M1
18	Maxillary molar alveolar length (Molar_alveolar_Ln)	P^4/M^1 buccal alveolar crest to distal M^3 buccal alveolar crest	Surrogate for mesiodistal length of molar crowns, related to tooth crown strength (resistance to ribbon fractures), rate of wear, and occlusal area	P4-M1:DM3
19	Maxillary canine alveolar length (Canine_Ln)	C^1/P^3 buccal alveolar crest to I^2/C^1 buccal alveolar crest (or mesial C^1 buccal alveolar crest if diastema is present)	Correlate of social signaling and possibly gape insofar as canine crown base dimensions may be correlated with canine projection	C-P3:MC
20	Maxillary bilateral incisor alveolar length (Bilat_Incisor)	Breadth between right and left C^1/I^2 buccal alveolar crests (or distal I^2 buccal alveolar crests if diastema is present)	Functional surface for incision	DI2_left:DI2_right
21	Postglenoid process to mandibular fossa (PG_MF)	Tip of postglenoid process to nadir of mandibular fossa in the same parasagittal plane	Related to articular eminence angle; surrogate for depth and inclination of the articular eminence, which should be correlated with the orientation of the joint reaction force at the TMJ	PG:MF
22	Mandibular fossa to articular eminence (MF_AE)	Nadir of mandibular fossa to apex of articular eminence in the same parasagittal plane as tip of postglenoid process	Related to articular eminence angle; surrogate for depth and inclination of the articular eminence, which should be correlated with the orientation of the joint reaction force at the TMJ	MF:AE
23	Postglenoid process to articular eminence (PG_AE)	Tip of postglenoid process to apex of articular eminence in the same parasagittal plane	Related to articular eminence angle; surrogate for depth and inclination of the articular eminence, which should be correlated with the orientation of the joint reaction force at the TMJ	PG:AE
24	Articular eminence to ectomolare2 (AE_EM2)	Apex of articular eminence to the buccal alveolar margin centered above M^2 (ectomolare2)	Approximates the M^2 load arm	AE:EM2
25	Articular eminence to ectopremolare4 (AE_EP4)	Apex of articular eminence to the buccal alveolar margin centered above P^4 (ectopremolare4)	Approximates the P^4 load arm	AE:EP4
26	Articular eminence to prosthion (AE_P)	Apex of articular eminence to the buccal alveolar margin centered between I^1s (prosthion)	Approximates the I^1 load arm	AE:P
27	Mechanical palate protrusion (Palate_Protrusion)	Articular eminence to prosthion (26) minus articular eminence to mid-zygomaticoalveolar crest	Moment arm of rostrum when bent/sheared in sagittal plane at incisors	AE:P - AE:ZAC
28	Inner palate breadth at P^3 (Br_palate_P3)	Breadth between lingual alveolar margins at mid-P^3 (entopremolare3)	Resistance to torsion during premolar bites	NP3_right:NP3_left
29	Inner palate breadth at M^2 (Br_Palate_M2)	Breadth between lingual alveolar margins at mid-M^2 (entomolare2)	Related to the triangle of support (narrow tooth rows allow higher maximum bite force in bites in Zone II)	NM2_right:NM2_left
Mandible				
1	Mandibular bicondylar breadth (Bicondyle_Br)		Related to triangle of support (widely separated	CS_right:CS_left

(*continued on next page*)

Table 2 (*continued*)

Measurement		Definition	Mechanical significance	Landmarks in SOM Table S1
		Breadth between superiormost points on right and left mandibular condyles (condylion superiore)	condyles allow higher maximum bite force in bites in Zone II)	
2	Mandibular condyle to ipsilateral M_3 (Condyle_M3)	Superior point of condyle (condylion superiore) to center of occlusal surface of ipsilateral M_3	M_3 load arm; related to ramus height above the occlusal plane	CS:NM3O
3	Mandibular condyle to ipsilateral M_1 (Condyle_M1)	Superior point of condyle (condylion superiore) to center of occlusal surface of M_1	M_1 load arm; related to ramus height above the occlusal plane	CS:NM1O
4	Ramus height above occlusal plane (Ramus_Ht_Occlusal)	Projected height of condylion superiore above the occlusal plane	Related to inclination of the triangle of support, which affects reduction of balancing side muscle force during bites in Zone II	Calculate with laws of cosine and sine using CS: NM3O, CS: NM1O, NM1O: NM3O
5	Intercorpus breadth at P_3 (Inter_P3_Br)	Breadth between lingual alveolar margins at mid-P_3 (entopremolare3)	Inversely proportional to torsional stress at mandibular symphysis during premolar bites	NNP3_right:NNP3_left
6	Intercorpus breadth at M_2 (Inter_M2_Br)	Breadth between lingual alveolar margins at mid-M_2 (entomolare2)	Related to triangle of support (narrow tooth rows allow higher maximum bite force in bites in Zone II)	NNM2_right:NNM2_left
7	Symphyseal height (Sym_Ht)	Median point of septum between the central incisors (labial I_1/I_1) to inferiormost point on median plane of symphysis (menton)	Resistance to shear in sagittal plane	LII:M
8	Maximum perpendicular symphyseal breadth (Sym_Br)	Breadth between points on labial and lingual sides of symphysis (symphysis outer, symphysis inner) that describe a chord presenting the maximum breadth of the symphysis perpendicular to the long axis of the symphyseal cross-section	Resistance to wishboning in transverse plane	SO:SI
9	Corpus height at M_2 (M2_Corp_Ht)	Corpus superior M_2 to inferiormost point on corpus directly inferior to M_2 (corpus inferior M_2)	Resistance to bending in sagittal plane at M_2	CRS:CI
10	Maximum perpendicular corpus breadth at M_2 (M2_Corp_Br)	Breadth between points corpus outer and corpus inner on buccal and lingual sides of corpus below M_2 that describe a chord presenting the maximum breadth of the corpus perpendicular to the long axis of the corpus cross-section	Related to corpus shape at M_2; resistance to torsion along corpus long axis and/or to bending stress in transverse plane at M_2	CO:CIN
11	Maximum P_4 breadth (P4_Br)	Maximum buccolingual chord distance between buccalmost and lingualmost points on P_4 crown	Related to tooth crown strength (resistance to ribbon fractures), rate of wear, and occlusal area	BNP4:LNP4
12	Maximum M_2 breadth (M2_Br)	Maximum buccolingual chord distance between buccalmost and lingualmost points on M_2 crown	Related to tooth crown strength (resistance to ribbon fractures), rate of wear, and occlusal area	BNM2:LNM2
13	Mandibular premolar alveolar length (PM_alveolar_Ln)	C_1/P_3 buccal alveolar crest to P_4/M_1 buccal alveolar crest	Surrogate for mesiodistal length of premolar crowns, related to tooth crown strength (resistance to ribbon fractures), rate of wear, and occlusal area	NC-P3:NP4-M
14	Mandibular molar alveolar length (Molar_alveolar_Ln)	P_4/M_1 buccal alveolar crest to distal M_3 buccal alveolar crest	Surrogate for mesiodistal length of molar crowns, related to tooth crown strength (resistance to ribbon fractures), rate of wear, and occlusal area	NP4-M:DNM3
15	Mandibular canine alveolar length (Canine_Ln)	C_1/P_3 buccal alveolar crest to I_2/C_1 buccal alveolar crest	Correlate of social signaling, and possibly gape insofar as canine crown base dimensions may be correlated with canine projection	MNC:DNMC
16	Mandibular bilateral incisor alveolar length (Bilat_Incisor)	Breadth between right and left C_1/I_2 buccal alveolar crests	Functional surface for incision	DNI2_right:DNI2_left
17	Ramus height (Ramus_Ht)	Nadir of mandibular notch to inferiormost point on ramus (pregonial tubercle)	Related to ramus area; proportional to cross sectional area of superficial and deep masseter	MN:PT
18	Anterioposterior breadth of ramus at occlusal plane (Ramus_Br)	Distance between anteriormost and posteriormost points of ramus in occlusal plane (anterior ramus, posterior ramus)	Related to ramus area; proportional to cross	AR:PR

Table 2 (*continued*)

Measurement		Definition	Mechanical significance	Landmarks in SOM Table S1
			sectional area of superficial and deep masseter	
19	Corpus height at M_1 (M1_Corp_Ht)	Corpus superior M_1 to inferiormost point on corpus directly inferior to M_1 (corpus inferior M_1)	Resistance to bending in sagittal plane at M_1	CSM1:CIM1
20	Maximum perpendicular corpus breadth at M_1 (M1_Corp_Br)	Breadth between points corpus outer and corpus inner on buccal and lingual sides of corpus below M_1 that describe a chord presenting the maximum breadth of the corpus perpendicular to the long axis of the corpus cross-section	Related to corpus shape at M_1; resistance to torsion along corpus long axis and/or to bending stress in transverse plane at M_1	COM1:CINM1

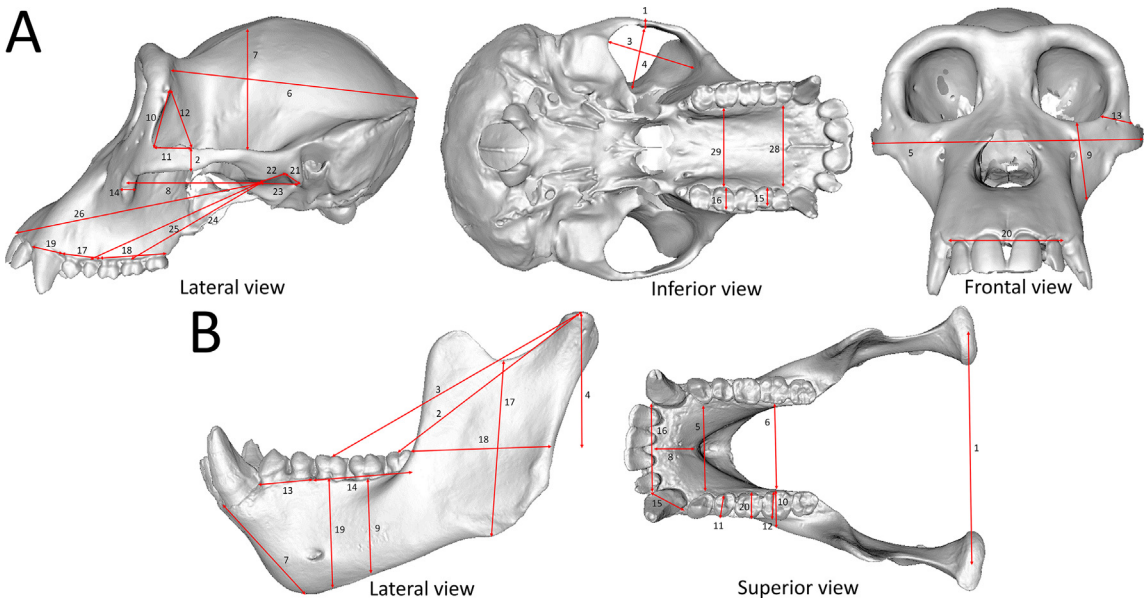

Figure 2. Craniometric measurements on the cranium and mandible (see Table 2 and SOM Table S1). A: cranium; B: mandible. Measurement of mechanical palate protrusion is not shown.

landmark data: 1) the functional interpretation of our biomechanically informative variables is tied directly to the linear dimensions (Table 2) and 2) interlandmark distances avoided statistically induced trait covariances that can occur due to Procrustes superimposition (i.e., the 'Pinocchio effect'; von Cramon-Taubadel et al., 2007; Zelditch et al., 2012; Goswami et al., 2019). All landmark data were collected by a single individual (H.J.). We estimated the midline or bilaterally absent landmarks using the thin-plate spline (TPS) method (Bookstein, 1989; Gunz et al., 2009; Baken et al., 2021) in the 'estimate.missing' function in the 'geomorph' package. The TPS process was applied within each genus independently and separately for males and females in *Gorilla* due to their distinct morphologies, such as strongly developed crests and larger canines in the male gorilla cranium. In *P. troglodytes*, 101 crania and 98 mandibles were used to maximize the sample size for missing landmark estimation as the TPS process was conducted for both sexes simultaneously, but 20 crania and 19 mandibles were later excluded in the analyses due to missing sex information (Table 1). We further explored the effects of pooling sex on TPS estimation in the human crania and found that variance in each linear measurement was not significantly different whether the TPS was performed with the two sexes combined or in separation (SOM S1).

To assess the intraobserver measurement error, the landmark protocol was collected five times from three crania and mandibles in each taxon, with at least one week between the trials. Error for each interlandmark distance was assessed using coefficient of variation (CV) to reflect the scale of measurement (Sokal and Rohlf, 2001: 57–59). The mean CV for the three species was $\leq$1.59% and $\leq$1.05% in the cranium and mandible, respectively, which is within acceptable levels ($\leq$5%; White and Folkens, 2000).

However, we also observed a negative correlation between the means and CVs of the linear dimensions across the five trials for the full measurement set, i.e., larger traits tended to be measured with greater repeatability. The average correlation across all the five trials was −0.56 for the cranium and −0.37 for the mandible. We therefore further measured the two largest (maximum length of temporalis origin, bi-zygomatic breadth) and the two smallest (breadth of midzygomatic arch, minimum thickness of zygomatic root) measurements in the cranium 20 times in one chimpanzee cranium with at least 3 days between the trials. The error for the large dimensions was 0.265 mm (CV = 0.22%) in maximum length of temporalis origin and 0.125 mm (CV = 0.1%) in bi-zygomatic breadth, and that for small dimensions was 0.029 mm (CV = 1.3%) in breadth of midzygomatic arch and 0.061 mm (CV = 1.08%) in minimum thickness of zygomatic root. This confirms that absolutely smaller measurements have higher relative variance (i.e., CV) on average, which likely reflects measurement error and resolution, even given absolutely smaller measurement errors (discretization of the distribution inflates variance of measurements with smaller

means; Rohlf et al., 1983). We discuss the impact of this issue on our interpretation of the evolvability statistics in the following.

Species-specific phenotypic variance/covariance (P) matrices of the biomechanically significant linear measurements of a 29-variable set for the cranium and a 20-variable set for the mandible, respectively, were generated using raw measurements (form data) and raw measurements scaled by the geometric mean of the traits (shape data) for the cranium and mandible. We chose to correct for size via scaling by the geometric mean to preserve geometric similarity (i.e., isometric variants are identical after size correction) and control the intrageneric and intergeneric size variation (Jungers et al., 1995). Multivariate analysis of variance indicates significant sex differences in all the three genera and subspecies differences in *Pan*. To correct for sex variation (and subspecies variation in *P. troglodytes*), the vector of mean differences between males and females $\times$ 0.5 was subtracted from the males and added to the females in the sample, respectively (see Marroig and Cheverud, 2004, and Rolian, 2009 for a similar approach). This procedure was utilized for the form and shape datasets.

2.3. Analytical methods

Patterns of integration captured by phenotypic variance/covariance matrices As detailed in the following, we compared the patterns of integration captured by P matrices by 1) obtaining the angle between the first principal component (PC 1) of each species as calculated from their respective P matrices and 2) calculating random skewers (Cheverud and Marroig, 2007). We chose not to use common principal component analysis (Flury, 1988; Phillips and Arnold, 1999), which is often used for this purpose, as Pepler et al. (2016) suggest that substantially larger sample sizes are required to produce reliable results using this method. However, the results of common principal component analysis (CPC) can be found in SOM S1 and SOM Tables S2–S4 for interested readers.

The genotypic variance/covariance (G) and P matrices often demonstrate conserved characteristics, particularly eigenvectors, although these matrices can evolve via selection and drift (Steppan et al., 2002; Arnold et al., 2008). The PC 1 axis may be more stable than the higher PC axes because PC 1 reflects the axis of form or shape variation accounting for the most variation (i.e., g_{max} or p_{max}). Thus, the angles between the PC 1 axes from species-specific PCAs were calculated as the arccosine of the absolute value of the dot product of the normalized PC 1 eigenvectors. This produces angles ranging from 0° (identical shape changes) to 90° (uncorrelated shape changes). The null hypothesis of no correlation between PC 1 axes was tested as follows: 1) 10,000 normalized random vectors were generated; 2) the absolute value of correlation was calculated between a pair of random vectors resampled without replacement from these 10,000 random vectors; 3) step 2 was repeated 999 times; and 4) the null hypothesis of no correlation between the species' PC 1 axes was rejected if the observed correlation between the PC 1 axes exceeded 95% of the 1000 permuted absolute value of correlations between the random vectors. We also tested whether the angle between the PC 1 axes for each pair of species is significantly different from that between the other species pairs: 1) specimens were resampled with replacement (i.e., bootstrapping) from each species equal to the sample size of that species; 2) the PCA was performed on the covariance matrices of the bootstrapped samples, and the angle between their respective PC 1 axes was calculated; 3) step 2 was repeated 999 times for each species pair; and 4) a two-tailed t-test was used to compare the bootstrapped angles from each resampled species pair at $\alpha = 0.05$. This was used to test, for example, whether the angle between the PC 1 axes in *P. troglodytes* and *G. gorilla* was significantly different from the angle between the PC 1 axes in *P. troglodytes* and *H. sapiens*.

The method of random skewers measures how populations respond to selection by calculating the mean vector correlation between response vectors that result from the application of random unit selection vectors ('random skewers') to two P matrices (i.e., P matrix similarity; Cheverud, 1996; Cheverud and Marroig, 2007; Melo et al., 2015). Random skewers is based on the breeder's equation (or Lande equation): $\Delta z = G\beta$, where Δz is the evolutionary change in a vector of trait means, β is the selection gradient, and G is the additive genetic variance/covariance matrix (Lande, 1979). We substitute P for G, which is appropriate if the matrices are equal or proportional within populations. G and P are often very similar across primate species (e.g., Roff, 1995; Cheverud, 1996; de Oliveira et al., 2009), including recent humans (Martínez-Abadías et al., 2012). We used 10,000 normalized random selection vectors. The null hypothesis of no structural similarity between two P matrices is rejected if the observed correlation between response vectors is above the 95th percentile of the distribution of correlations between random vectors (Cheverud et al., 1983; Cheverud, 1996). Random skewers were calculated using the 'RandomSkewers' function in the 'evolqg' package v. 0.2-9. (Melo et al., 2015) in R v. 4.1.1.

Examining common structures in multivariate trait variance and covariance is complex, and there is no single statistic or method that neatly captures all relevant parameters. We use two approaches to comparing P matrices across extant species as there are limitations in each of these methods. For example, the angle between the PC 1 axes may not be informative for comparing the patterns of P matrices if the first two eigenvalues are similar and PC axes become 'swapped.' Moreover, the angle between the PC 1 axes relies on eigen decomposition of covariance matrices (i.e., PCA), but biological interpretation of PC axes is not straightforward. Causes of covariance structure in populations are not constrained to be orthogonal, and any change to a single causal factor may affect all PC axes, which may affect the angle between the PC 1 axes. Regarding random skewers, Rohlf (2017) pointed out that it is difficult to interpret mean values of the angles between response vectors when they are intermediate as the underlying distribution of values may be bimodal. Given these challenges, we apply a complementary approach to the problem by computing trait-wise evolutionary statistics.

Trait-wise comparisons using evolutionary statistics We also consider whether trait variation and covariation might similarly influence evolutionary change in hominines by calculating (unconditional) evolvability (e), conditional evolvability (c), and integration (i) values for each trait (sensu Hansen and Houle, 2008). These measures summarize the evolutionary potential of a trait or its potential, given its covariance with other traits captured by the P matrix. For this calculation, the P matrix was mean standardized by the product of the trait mean vector in each species in order to measure the expected proportional response per generation per unit directional selection (Hansen and Houle, 2008). This procedure ensures that larger traits do not necessarily result in larger evolutionary responses. Many studies present average e, c, and i values calculated for the entire P matrix, but the trait-level calculations presented here are better for comparing overall patterns across taxa, which is one of the major aims of this study. The average multivariate measures of evolutionary responses to the selection gradient acting on the P matrix are presented in SOM S1 and SOM Table S5 for interested readers.

When calculated on a trait-by-trait basis, e is the variance of that trait and c is the inverse of the corresponding diagonal element of P^{-1} (Hansen and Houle, 2008). These evolvability statistics measure the available variation on which selection can act (i.e., evolutionary

potential) with or without accounting for constraints due to covariation with other traits (c and e, respectively). In this context, integration is the reduction in evolvability after accounting for conditioning on other traits and is calculated as $i = 1 - ([P^{-1}]_{jj}[P]_{jj})^{-1}$, where $[P]_{jj}$ signifies the jjth element of the P matrix. Thus, the value of i ranges between 0 and 1, representing complete independence to perfect correlation with other traits, respectively. This measure of integration is the inverse of the more commonly reported autonomy (a) statistic, where $a = ([P^{-1}]_{jj}[P]_{jj})^{-1}$. Autonomy is therefore the proportion of variance independent from all other traits. We then calculated the Pearson correlation coefficient between the vectors of e, c, or i values for species pairs within each dataset. This provides a rough measure of how similarly these values are patterned across species. The same bootstrapping method and a two-tailed t-test described above were used to compare trait-wise evolutionary statistics and their Pearson correlation coefficients from each resampled species pair at $\alpha = 0.05$.

As discussed previously, traits with smaller means have proportionally higher variances (i.e., there is a negative relationship between trait means and CVs). This means that particularly small dimensions have inflated variances after mean standardization, which is problematic for the interpretation of measures of variability such as evolvability and integration. For this reason, trait-wise evolutionary statistics can be compared between species, or among similarly scaled dimensions, but not between traits of different scales (see also Hansen and Houle, 2008; Grabowski et al., 2011).

Magnitude of integration In addition to comparing patterns of variation, the relative eigenvalue variance (V_{rel}) and integration coefficient of variation (ICV) were calculated for each P matrix to compare the magnitude or strength of integration across the three species. Eigenvalue variance is the average squared deviation of the eigenvalues from the mean eigenvalue. The V_{rel} scales eigenvalue variance by the theoretical maximum eigenvalue variance calculated as $V_{rel} = \frac{\sum(\lambda_i - \bar{\lambda})^2}{p(p-1)\bar{\lambda}^2}$, where λ_i is the eigenvalue of the ith eigenvector, $\bar{\lambda}$ is the mean of eigenvalues, and p is the number of nontrivial (i.e., where $\lambda > 0$) eigenvalues for the trait covariance matrix (Pavlicev et al., 2009; Conaway and Adams, 2022), whereas the ICV scales eigenvalue variance by the mean of all eigenvalues (Shirai and Marroig, 2010). In both cases, higher values indicate that most of the variation is tied up in only a few dimensions (i.e., the group is highly integrated). Following Conaway and Adams (2022), the V_{rel} was linear-transformed (V^*_{rel}) so that its range matches the bivariate correlation coefficient (−1 to +1). Next, V^*_{rel} was Z-transformed as the standardized effect size (Z_{Vrel}): $Z_{Vrel} = \frac{1}{2}\ln\left(\frac{1+V^*_{rel}}{1-V^*_{rel}}\right)$. This procedure makes not only the distribution of Z_{Vrel} normal across the range of V_{rel} but also the variance in the sampling distribution relatively constant (Conaway and Adams, 2022). Then, Z_{Vrel} can be directly compared using the two-sample test statistic: $\hat{Z}_{12} = \frac{|Z_1 - Z_2|}{\sqrt{\sigma^2_{Z_1} + \sigma^2_{Z_2}}}$ (Conaway and Adams, 2022). The V_{rel} values and their effect size were calculated and compared using the 'integration.Vrel' and 'compare.ZVrel' functions, respectively, in the 'geomorph' package v. 4.0.4. (Baken et al., 2021) in R v. 4.1.1. The ICV values were calculated using the 'MeanMatrixStatistics' function in the 'evolqg' package v. 0.2-9. (Melo et al., 2015) in R v. 4.1.1. The same bootstrapping method and the two-tailed t-test described previously were used to compare ICV values from each resampled species pair at $\alpha = 0.05$.

3. Results

3.1. Patterns of integration—Principal component analysis

Cranial form Standard PCA was conducted on each species' P matrix of unscaled dimensions (form data). The first PC explained 35% of variation in *Homo*, 45% in *Pan*, and 45% in *Gorilla*. The angle between the PC 1 axes based on raw cranial dimensions was the smallest between *Pan* and *Gorilla* (11.3°) and the largest between *Homo* and *Pan* (29.1°; $p < 0.05$; Table 3). Angles in this range indicate highly correlated shape changes captured by PC 1 (equivalent to Pearson's $r \geq 0.87$; $p < 0.05$). Length and height of the temporalis muscle (traits 6 and 7) loaded heavily on PC 1 in all taxa, but particularly in *H. sapiens*. Facial projection ahead of the articular eminence (traits 8, 24, 25, and 26) and bizygomatic breadth (trait 5) also had high positive loadings for all three species, but more so for the African apes (Table 4; Fig. 3).

Cranial shape Standard PCA was conducted on each species' P matrix of size-scaled dimensions. The first PC explained 31% of variation in *Homo*, 29% in *Pan*, and 27% in *Gorilla*. The angles between the PC 1 axes ranged from 51.4° between *Pan* and *Gorilla* to 86.7° between *Homo* and *Pan*. The primary patterns of cranial shape variation are thus more divergent among the three species than for the form data (Table 3; Fig. 4). The maximum length and height of the temporalis (traits 6 and 7) loaded most heavily in both *H. sapiens* and *G. gorilla* but did not contribute greatly to PC 1 in *P. troglodytes* (Table 4). Indeed, these two traits strongly dominate PC 1 in *H. sapiens*. Projection of the upper jaw and the anterior zygomatic arch ahead of the articular eminence (traits 8, 24, 25, and 26) load heavily in *P. troglodytes* and, to a lesser extent, in *G. gorilla*.

Table 3
Angle between the species-specific first principal component (PC 1) axes (with equivalent Pearson correlation coefficient in parentheses) and random skewers results in the cranium and mandible. All correlation coefficients are statistically significant ($p < 0.05$) against the null hypothesis of no correlation for angle between the PC 1 axes or no structural similarity for random skewers except *Homo sapiens-Pan troglodytes* comparison of the angle between the PC 1 axes.[a]

Skull region	Comparisons	Angle between PC 1 axes (°)		Random skewers (r)	
		Form data	Shape data[b]	Form data	Shape data[b]
Cranium	*H.s.–P.t.*	29.1 (0.87)*,$	86.7 (0.06)*,$	0.85	0.80
	H.s.–G.g.	23.3 (0.92)*,※	52.8 (0.61)*	0.88	0.81
	P.t.–G.g.	10.7 (0.98)$,※	51.4 (0.62)$	0.91	0.77
Mandible	*H.s.–P.t.*	24.1 (0.91)*,$	70.7 (0.33)*,$	0.84	0.81
	H.s.–G.g.	22.0 (0.93)*,※	56.6 (0.55)*,※	0.84	0.79
	P.t.–G.g.	11.1 (0.98)$,※	17.5 (0.95)$,※	0.94	0.92

Abbreviations: *H.s.* = *Homo sapiens*; *P.t.* = *Pan troglodytes*; *G.g.* = *Gorilla gorilla*.
[a] An asterisk (*) indicates statistically significant difference between *H.s.–P.t.* pair and *H.s.–G.g.* pair. A dollar sign ($) indicates statistically significant difference between *H.s.–P.t.* pair and *P.t.–G.g.* pair; A reference mark (※) indicates statistically significant difference between *H.s–G.g.* pair and *P.t–G.g.* pair. Statistically significant when $p < 0.05$.
[b] Shape data are the raw dimensions scaled by geometric mean of each individual.

Table 4
Loadings of each trait on the species-specific first principal component in the cranium and mandible.

Measurement[a]		Form data			Shape data[b]		
		H.s.	*P.t.*	*G.g.*	*H.s.*	*P.t.*	*G.g.*
Cranium							
1	Br_midzygo	−0.0111	0.0183	0.0061	−0.0167	−0.0420	−0.0249
2	Ht_midzygo	−0.0177	0.0238	0.0315	−0.0380	−0.0823	0.0100
3	MaxLn_tempfora	0.1324	0.1966	0.1899	0.0502	0.2561	0.2922
4	MaxBr_tempfora	0.1033	0.1584	0.1719	−0.0013	0.0336	0.2101
5	Bi_zygo	0.2565	0.4114	0.3671	0.0162	0.0903	0.2241
6	Temp_Ln	**0.6669**[c]	0.3322	0.4414	**0.7950**	0.1549	0.4223
7	Temp_Ht	0.5370	**0.4304**	**0.4423**	0.5802	0.0073	**0.4860**
8	AE_MT	0.1345	0.1794	0.1697	−0.0716	0.3532	0.1734
9	Zygomatico_exp	0.0492	0.1239	0.1219	−0.0021	0.0366	0.0572
10	FMT_J	0.0914	0.1185	0.0399	0.0595	−0.0260	−0.0482
11	J_ZAS	0.0333	0.0801	0.0402	−0.0159	0.1019	−0.0123
12	FMT_ZAS	0.1291	0.1267	0.1028	0.0764	0.0501	0.0355
13	PO_Br	0.0923	0.0969	0.1028	0.0392	−0.0363	0.1029
14	AZM_PR	0.0371	−0.0084	−0.0054	−0.0204	−0.0821	−0.1434
15	P4_Br	0.0235	0.0143	0.0154	−0.0037	0.0108	−0.0371
16	M2_Br	0.0163	0.0185	0.0107	−0.0102	0.0203	−0.0502
17	PM_alveolar_Ln	0.0266	0.0166	0.0143	−0.0036	0.0555	−0.0679
18	Molar_alveolar_Ln	0.0531	0.0396	0.0276	−0.0297	0.0753	−0.1323
19	Canine_Ln	0.0232	0.0819	0.0328	0.0032	0.0028	0.0645
20	Bilat_Incisor	0.0323	0.0785	0.0145	−0.0431	0.1245	−0.1396
21	PG_MF	0.0054	0.0322	0.0293	−0.0229	−0.0103	−0.0277
22	MF_AE	0.0172	0.0400	0.0185	0.0062	−0.1096	−0.0074
23	PG_AE	0.0258	0.0773	0.0521	0.0231	−0.1078	−0.0028
24	AE_EM2	0.1245	0.2629	0.2774	−0.0555	0.3607	0.3625
25	AE_EP4	0.1617	0.2757	0.2962	−0.0361	0.4416	0.2794
26	AE_P	0.2255	0.3984	0.3553	−0.0294	**0.5674**	0.2131
27	Palate_protrusion	0.0985	0.1916	0.1606	−0.0034	0.2045	0.1772
28	Br_palate_P3	0.0323	0.0842	0.0950	−0.0106	0.0463	−0.0075
29	Br_palate_M2	0.0755	0.0743	0.0887	0.0272	0.0726	0.0001
Mandible							
1	Bicondyle_Br	0.3262	0.2869	0.3223	**0.8046**	0.0173	0.2043
2	Condyle_M3	0.4222	**0.5250**	0.4892	0.3221	0.5573	**0.5776**
3	Condyle_M1	0.3705	0.4859	**0.4905**	0.3580	0.4163	0.5103
4	Ramus_Ht_Occlusal	**0.5345**	0.4539	0.3697	−0.0754	**0.6072**	0.5231
5	Inter_P3_Br	0.0403	0.0329	0.0906	0.0424	−0.0700	−0.0597
6	Inter_M2_Br	0.0545	0.0343	0.0654	0.2477	−0.0324	0.0540
7	Sym_Ht	0.0957	0.1674	0.2427	−0.0581	−0.0363	−0.0531
8	Sym_Br	0.0567	0.0497	0.0684	−0.0681	−0.0285	−0.0459
9	M2_Corp_Ht	0.2296	0.0955	0.1300	0.0398	−0.0039	−0.0578
10	M2_Corp_Br	0.0155	0.0161	0.0144	−0.1248	−0.0700	−0.0900
11	P4_Br	0.0116	0.0005	0.0029	−0.0012	−0.0306	−0.0264
12	M2_Br	0.0191	0.0063	0.0051	0.0052	−0.0372	−0.0220
13	PM_alveolar_Ln	−0.0258	0.0034	0.0144	−0.0399	−0.0601	−0.0459
14	Molar_alveolar_Ln	0.0792	−0.0235	0.0444	0.0306	−0.1659	−0.0247
15	Canine_Ln	−0.0130	0.0677	0.0157	−0.0227	−0.0659	−0.0476
16	Bilat_Incisor	0.0180	0.0087	0.0162	−0.0110	−0.1046	−0.0525
17	Ramus_Ht	0.4119	0.2339	0.2934	0.1036	0.1925	0.1410
18	Ramus_Br	0.0471	0.2898	0.2550	0.0314	0.2139	0.1744
19	M1_Corp_Ht	0.2067	0.1126	0.1727	0.0010	−0.0072	−0.0507
20	M1_Corp_Br	0.0008	0.0329	0.0507	−0.1090	−0.0503	−0.0770

Abbreviations: *H.s.* = *Homo sapiens*; *P.t.* = *Pan troglodytes*; *G.g.* = *Gorilla gorilla*.
[a] See Table 2 for abbreviations of linear measurements.
[b] Shape data are the raw dimensions scaled by geometric mean of each individual.
[c] Highest PC loadings are bolded.

In comparison, facial projection loads weakly and negatively on the *H. sapiens*' PC 1.

Mandible form The PC 1 explained 28% of variation in *Homo*, 44% in *Pan*, and 46% in *Gorilla*. The angle between the PC 1 vectors was significantly smaller between *Pan* and *Gorilla* for the mandible form (11.1°) and was the largest between *Homo* and *Pan* (24.1°; $p < 0.05$), but all angles suggest strong correlation of form changes along this axis ($r > 0.90$; Table 3). There was a large degree of overlap in traits that loaded strongly on PC 1 for the mandible form in all the three hominoid species, including ramus height above the occlusal plane (trait 4), distance from the condyle to the molars (traits 2 and 3), and bicondylar breadth (trait 1; Table 4; Fig. 3). Ramus breadth (trait 18) contributes more strongly in the two African apes than in humans.

Mandible shape The PC 1 explained 31% of variation in *Homo*, 31% in *Pan*, and 39% in *Gorilla*. The primary axis of mandible shape variation is nearly identical in the two African ape species (17.5°) but still moderately correlated between humans and the two ape species (56.6–70.7°; Table 3). Some of the same traits that loaded strongly in the PCA of mandible form in all the three taxa also do so in the PCA of mandible shape, including the distance of the condyle to M_1/M_3 (traits 2 and 3; Table 4; Fig. 4). Bicondylar breadth (trait 1) is the trait that loads most strongly in *H. sapiens* and also contributes considerably to PC 1 in *G. gorilla* but does not contribute

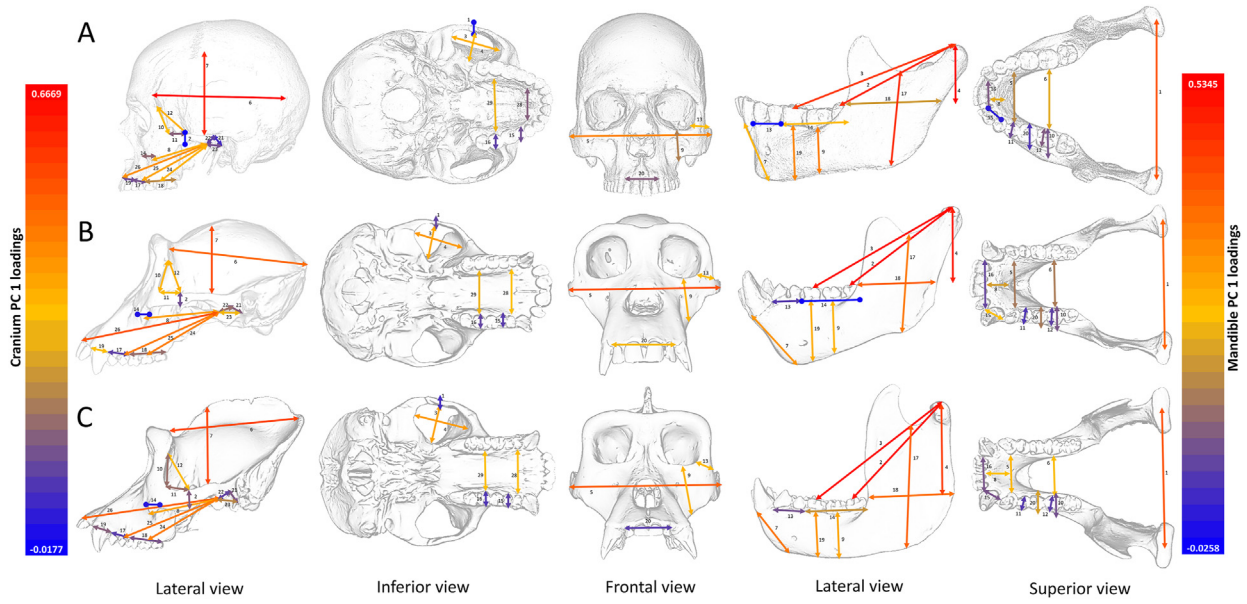

Figure 3. A visualization of the first principal component (PC 1) axis in the form data. The A) human, B) chimpanzee and C) gorilla cranium and mandible in lateral view are aligned in Frankfort horizontal and molar occlusal planes, respectively. Positive and negative PC 1 loadings are presented with arrows and lines with circles, respectively. Red and blue colors show high and low PC 1 loadings, respectively. Measurement of mechanical palate protrusion is not shown. (For interpretation of the references to color in this figure legend, the reader is referred to the web version of this article.)

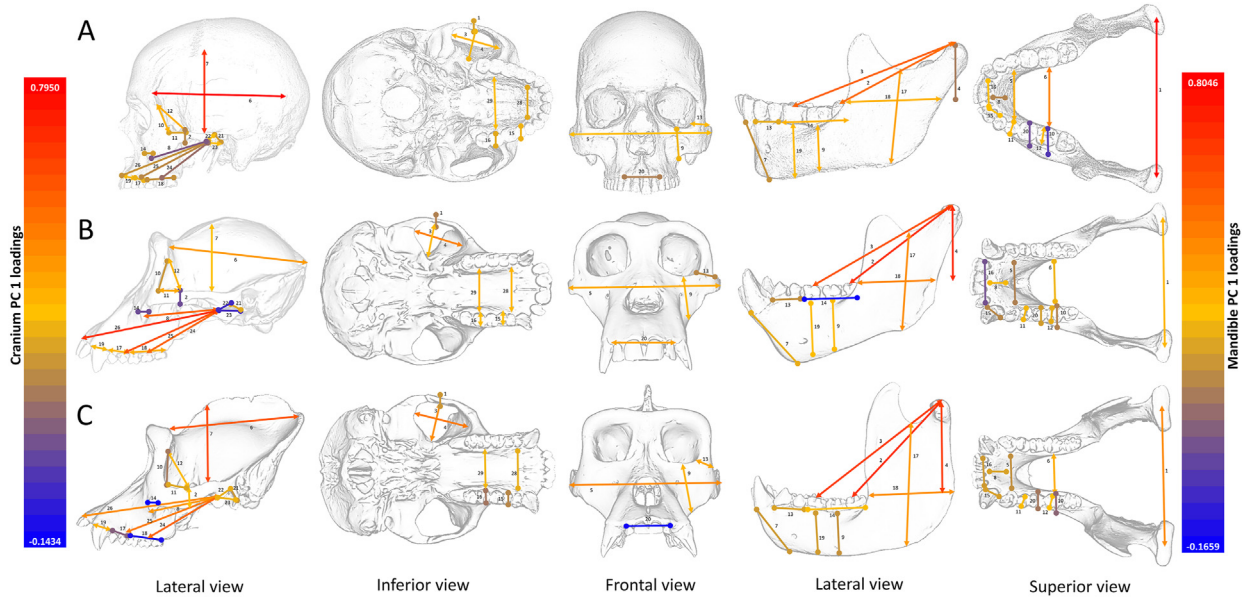

Figure 4. A visualization of the first principal component (PC 1) axis in the shape data. The A) human, B) chimpanzee and C) gorilla cranium and mandible in lateral view are aligned in Frankfort Horizontal and molar occlusal planes, respectively. Positive and negative PC 1 loadings are presented with the arrows and lines with circles, respectively. Red and blue colors show high and low PC 1 loadings in the cranium and mandible, respectively. Measurement of mechanical palate protrusion is not shown. (For interpretation of the references to color in this figure legend, the reader is referred to the web version of this article.)

meaningfully in *P. troglodytes*. Intercorpus breadth at the M_2s (trait 6) also loads heavily on PC 1 in *H. sapiens*, whereas ramus breadth (trait 18) and particularly ramus height above the occlusal plane (trait 4) load more strongly on PC 1 in the African ape species.

3.2. Patterns of integration—Random skewers

The random skewers analysis indicated that correlations between pairs of taxa were statistically significant for all comparisons in the cranium and mandible ($p < 0.05$). Correlations ranged from 0.84 to 0.94 for the form data and from 0.77 to 0.92 for the shape data (Table 3). Overall, the form data showed higher correlations than the shape data, consistent with the results from the angle between PC 1 axes discussed previously (Table 3).

3.3. Trait-wise comparison of evolutionary statistics

The Pearson correlation between the species vectors of e or c values allows comparison of trait evolvability among taxa. The species correlations for e and c in the cranial form (unscaled and

Table 5
Pearson correlation coefficient of trait-wise evolvability, conditional evolvability, and integration values between taxa. All Pearson correlation coefficients are statistically significant ($p < 0.05$) against the null hypothesis of no correlation.[a]

Skull region	Comparisons	Evolvability (e)		Conditional evolvability (c)		Integration (i)	
		Form	Shape	Form	Shape	Form	Shape
Cranium	*H.s.-P.t.*	$0.84^{*,\$}$	$0.82^{\$}$	$0.90^{*,\$}$	$0.85^{*,\$}$	$0.63^{*,\$}$	$0.61^{*,\$}$
	H.s.-G.g.	$0.86^{*,※}$	$0.81^{※}$	$0.95^{*,※}$	$0.81^{*,※}$	$0.68^{*,※}$	$0.53^{*,※}$
	P.t.-G.g.	$0.97^{\$,※}$	$0.90^{\$,※}$	$0.96^{\$,※}$	$0.90^{\$,※}$	$0.84^{\$,※}$	$0.71^{\$,※}$
Mandible	*H.s.-P.t.*	$0.80^{*,\$}$	$0.82^{*,\$}$	$0.78^{*,\$}$	0.83^{*}	$0.74^{*,\$}$	$0.62^{*,\$}$
	H.s.-G.g.	$0.70^{*,※}$	$0.76^{*,※}$	$0.46^{*,※}$	$0.85^{*,※}$	$0.83^{*,※}$	0.67^{*}
	P.t.-G.g.	$0.44^{\$,※}$	$0.58^{\$,※}$	$0.57^{\$,※}$	$0.82^{※}$	$0.92^{\$,※}$	$0.72^{\$}$

Abbreviation: *H.s = Homo sapiens*; *P.t = Pan troglodytes*; *G.g = Gorilla gorilla*.
[a] An asterisk (*) indicates statistically significant difference between *H.s.–P.t.* pair and *H.s.–G.g.* pair. A dollar sign ($) indicates statistically significant difference between *H.s.–P.t.* pair and *P.t.–G.g.* pair; A reference mark (※) indicates statistically significant difference between *H.s–G.g.* pair and *P.t–G.g.* pair. Statistically significant when $p < 0.05$.

Table 6
Trait-wise evolvability, conditional evolvability, and integration in the form data of cranium and mandible.

Measurement[a]		Evolvability (e)[b]			Conditional evolvability (c)[b]			Integration (i)			Autonomy (a)		
		H.s.	*P.t.*	*G.g.*	*H.s.*	*P.t.*	*G.g.*	*H.s.*	*P.t.*	*G.g.*	*H.s.*	*P.t.*	*G.g.*
Cranium													
1	Br_midzygo	**3.695**[c]	9.254	**8.159**	**2.489**	4.471	**3.603**	0.326	0.517	0.558	**0.674**	0.483	0.442
2	Ht_midzygo	2.783	4.939	2.248	1.343	2.086	0.981	0.517	0.578	0.564	0.483	0.422	0.436
3	MaxLn_tempfora	0.441	0.519	0.664	0.136	0.094	0.120	0.693	0.819	0.819	0.307	0.181	0.181
4	MaxBr_tempfora	0.797	0.850	0.767	0.441	0.134	0.122	0.447	0.842	0.841	0.553	0.158	0.159
5	Bi_zygo	0.132	0.264	0.216	0.043	0.026	0.030	0.677	0.900	0.860	0.323	0.100	0.140
6	Temp_Ln	0.276	0.292	0.435	0.133	0.084	0.191	0.518	0.713	0.560	0.482	0.287	0.440
7	Temp_Ht	0.551	0.629	0.668	0.218	0.158	0.204	0.604	0.749	0.695	0.396	0.251	0.305
8	AE_MT	0.447	0.472	0.435	0.122	0.048	0.055	0.726	0.899	0.874	0.274	0.101	0.126
9	Zygomatico_exp	0.626	0.579	0.530	0.406	0.244	0.183	0.351	0.578	0.654	0.649	0.422	0.346
10	FMT_J	0.735	1.472	1.596	0.115	0.299	0.276	0.844	0.797	0.827	0.156	0.203	0.173
11	J_ZAS	3.129	0.954	1.907	0.564	0.281	0.643	0.820	0.706	0.663	0.180	0.294	0.337
12	FMT_ZAS	0.545	0.879	0.933	0.060	0.153	0.124	0.891	0.826	0.867	0.109	0.174	0.133
13	PO_Br	1.461	0.868	1.082	0.422	0.238	0.245	0.711	0.726	0.773	0.289	0.274	0.227
14	AZM_PR	3.222	**10.273**	7.745	1.589	**5.402**	2.904	0.507	0.474	0.625	0.493	**0.526**	0.375
15	P4_Br	0.461	0.497	0.337	0.179	0.145	0.127	0.613	0.709	0.624	0.387	0.291	0.376
16	M2_Br	0.511	0.583	0.326	0.261	0.164	0.119	0.491	0.719	0.636	0.509	0.281	0.364
17	PM_alveolar_Ln	0.600	0.581	0.395	0.236	0.263	0.188	0.607	0.548	0.524	0.393	0.452	0.476
18	Molar_alveolar_Ln	0.391	0.304	0.266	0.132	0.087	0.068	0.664	0.713	0.746	0.336	0.287	0.254
19	Canine_Ln	0.690	1.787	0.838	0.391	0.636	0.458	0.433	0.644	0.453	0.567	0.356	**0.547**
20	Bilat_Incisor	0.450	0.390	0.340	0.133	0.111	0.170	0.703	0.716	0.501	0.297	0.284	0.499
21	PG_MF	1.707	3.221	2.990	0.911	0.459	0.747	0.466	0.857	0.750	0.534	0.143	0.250
22	MF_AE	1.092	2.448	1.206	0.309	0.108	0.228	0.717	0.956	0.811	0.283	0.044	0.189
23	PG_AE	0.600	1.462	0.880	0.143	0.047	0.099	0.762	0.968	0.888	0.238	0.032	0.112
24	AE_EM2	0.400	0.425	0.426	0.027	0.012	0.012	0.932	**0.971**	0.971	0.068	0.029	0.029
25	AE_EP4	0.236	0.318	0.319	0.007	0.009	0.007	**0.969**	0.971	**0.977**	0.031	0.029	0.023
26	AE_P	0.150	0.234	0.208	0.007	0.009	0.007	0.955	0.961	0.965	0.045	0.039	0.035
27	Palate_Protrusion	0.362	0.475	0.387	0.073	0.056	0.045	0.799	0.881	0.884	0.201	0.119	0.116
28	Br_palate_P3	0.507	0.391	0.704	0.121	0.149	0.253	0.762	0.620	0.640	0.238	0.380	0.360
29	Br_palate_M2	0.321	0.458	0.602	0.104	0.190	0.195	0.678	0.585	0.676	0.322	0.415	0.324
Mandible													
1	Bicondyle_Br	0.217	0.427	0.436	0.133	0.217	0.231	0.384	0.491	0.470	0.616	0.509	0.530
2	Condyle_M3	0.271	0.484	0.417	0.009	0.003	0.002	**0.967**	**0.994**	**0.994**	0.033	0.006	0.006
3	Condyle_M1	0.157	0.286	0.278	0.005	0.002	0.002	0.966	0.992	0.993	0.034	0.008	0.007
4	Ramus_Ht_Occlusal	**1.865**	**1.667**	0.791	0.461	0.209	0.056	0.753	0.874	0.929	0.247	0.126	0.071
5	Inter_P3_Br	0.563	0.381	0.969	0.156	0.152	**0.412**	0.723	0.601	0.575	0.277	0.399	0.425
6	Inter_M2_Br	0.370	0.310	0.556	0.138	0.168	0.288	0.627	0.459	0.481	0.373	0.541	0.519
7	Sym_Ht	0.689	0.671	0.701	0.294	0.172	0.184	0.573	0.744	0.737	0.427	0.256	0.263
8	Sym_Br	1.258	0.907	0.865	**0.631**	**0.531**	0.308	0.498	0.415	0.645	0.502	0.585	0.355
9	M2_Corp_Ht	0.767	0.489	0.688	0.092	0.063	0.081	0.880	0.871	0.883	0.120	0.129	0.117
10	M2_Corp_Br	1.430	0.709	0.758	0.294	0.204	0.206	0.794	0.712	0.729	0.206	0.288	0.271
11	P4_Br	0.431	0.655	0.535	0.192	0.333	0.229	0.553	0.492	0.572	0.447	0.508	0.428
12	M2_Br	0.346	0.492	0.318	0.105	0.227	0.102	0.696	0.539	0.679	0.304	0.461	0.321
13	PM_alveolar_Ln	0.617	0.444	0.297	0.209	0.229	0.126	0.662	0.483	0.576	0.338	0.517	0.424
14	Molar_alveolar_Ln	0.211	0.286	0.220	0.065	0.050	0.041	0.691	0.827	0.812	0.309	0.173	0.188
15	Canine_Ln	0.509	0.560	0.267	0.180	0.259	0.099	0.647	0.536	0.630	0.353	0.464	0.370
16	Bilat_Incisor	0.790	0.369	0.543	0.335	0.255	0.314	0.576	0.310	0.422	0.424	**0.690**	**0.578**
17	Ramus_Ht	0.693	0.644	0.370	0.459	0.257	0.190	0.338	0.601	0.487	**0.662**	0.399	0.513
18	Ramus_Br	0.454	0.590	0.437	0.200	0.201	0.182	0.559	0.660	0.583	0.441	0.340	0.417
19	M1_Corp_Ht	0.660	0.679	0.833	0.067	0.075	0.072	0.898	0.890	0.914	0.102	0.110	0.086
20	M1_Corp_Br	1.501	0.716	**1.181**	0.349	0.196	0.261	0.767	0.726	0.779	0.233	0.274	0.221

Abbreviations: *H.s. = Homo sapiens*; *P.t. = Pan troglodytes*; *G.g. = Gorilla gorilla*.
[a] See Table 2 for abbreviation of linear measurements.
[b] Multiplied by 10^2.
[c] Highest trait-wise evolvability, conditional evolvability, and integration values are bolded.

Table 7
Trait-wise evolvability, conditional evolvability, and integration in the shape data of cranium and mandible.

Measurement[a]		Evolvability (e)[b]			Conditional evolvability (c)[b]			Integration (i)			Autonomy (a)		
		H.s.	*P.t.*	*G.g.*	*H.s.*	*P.t.*	*G.g.*	*H.s.*	*P.t.*	*G.g.*	*H.s.*	*P.t.*	*G.g.*
Cranium													
1	Br_midzygo	**3.696**[c]	8.327	**11.653**	**0.302**	0.640	**0.599**	0.918	0.923	0.949	0.082	0.077	0.051
2	Ht_midzygo	2.670	4.582	2.488	0.286	**0.690**	0.471	0.893	0.850	0.811	0.107	0.150	0.189
3	MaxLn_tempfora	0.404	0.412	0.610	0.090	0.079	0.093	0.778	0.808	0.848	0.222	0.192	0.152
4	MaxBr_tempfora	0.622	0.589	0.720	0.186	0.133	0.105	0.701	0.773	0.853	0.299	0.227	0.147
5	Bi_zygo	0.084	0.119	0.117	0.035	0.030	0.034	0.587	0.748	0.705	0.413	0.252	0.295
6	Temp_Ln	0.249	0.220	0.298	0.111	0.089	0.160	0.555	0.595	0.462	**0.445**	0.405	**0.538**
7	Temp_Ht	0.454	0.329	0.486	0.126	0.137	0.142	0.724	0.583	0.707	0.276	0.417	0.293
8	AE_MT	0.325	0.433	0.336	0.085	0.045	0.053	0.738	0.897	0.842	0.262	0.103	0.158
9	Zygomatico_exp	0.532	0.374	0.390	0.193	0.214	0.144	0.636	0.426	0.631	0.364	**0.574**	0.369
10	FMT_J	0.642	1.043	1.534	0.081	0.182	0.161	0.874	0.826	0.895	0.126	0.174	0.105
11	J_ZAS	3.087	0.814	1.724	0.212	0.196	0.338	0.931	0.759	0.804	0.069	0.241	0.196
12	FMT_ZAS	0.456	0.658	0.831	0.056	0.154	0.120	0.877	0.766	0.855	0.123	0.234	0.145
13	PO_Br	1.300	0.456	0.961	0.199	0.187	0.182	0.847	0.590	0.810	0.153	0.410	0.190
14	AZM_PR	2.822	**9.481**	6.380	0.249	0.562	0.425	0.912	0.941	0.933	0.088	0.059	0.067
15	P4_Br	0.320	0.465	0.611	0.137	0.137	0.087	0.572	0.706	0.857	0.428	0.294	0.143
16	M2_Br	0.410	0.576	0.632	0.158	0.135	0.072	0.615	0.765	0.885	0.385	0.235	0.115
17	PM_alveolar_Ln	0.468	0.729	0.567	0.145	0.181	0.146	0.689	0.752	0.742	0.311	0.248	0.258
18	Molar_alveolar_Ln	0.291	0.346	0.568	0.093	0.064	0.063	0.679	0.816	0.889	0.321	0.184	0.111
19	Canine_Ln	0.550	1.324	2.661	0.162	0.330	0.518	0.705	0.750	0.805	0.295	0.250	0.195
20	Bilat_Incisor	0.370	0.427	0.421	0.082	0.108	0.100	0.778	0.746	0.763	0.222	0.254	0.237
21	PG_MF	1.560	2.762	2.741	0.234	0.370	0.310	0.850	0.866	0.887	0.150	0.134	0.113
22	MF_AE	0.973	1.954	1.137	0.155	0.103	0.185	0.841	0.947	0.837	0.159	0.053	0.163
23	PG_AE	0.550	1.002	0.686	0.096	0.038	0.079	0.826	0.962	0.885	0.174	0.038	0.115
24	AE_EM2	0.350	0.304	0.386	0.026	0.011	0.014	0.925	0.963	**0.965**	0.075	0.037	0.035
25	AE_EP4	0.188	0.251	0.206	0.007	0.009	0.007	**0.963**	**0.963**	0.964	0.037	0.037	0.036
26	AE_P	0.085	0.171	0.094	0.007	0.009	0.021	0.922	0.946	0.775	0.078	0.054	0.225
27	Palate_Protrusion	0.294	0.389	0.257	0.059	0.054	0.046	0.798	0.861	0.820	0.202	0.139	0.180
28	Br_palate_P3	0.459	0.362	0.495	0.085	0.111	0.207	0.815	0.692	0.581	0.185	0.308	0.419
29	Br_palate_M2	0.279	0.443	0.563	0.084	0.161	0.143	0.700	0.637	0.746	0.300	0.363	0.254
Mandible													
1	Bicondyle_Br	0.298	0.314	0.326	0.056	0.030	0.041	0.811	0.905	0.874	0.189	0.095	0.126
2	Condyle_M3	0.249	0.298	0.324	0.008	0.003	0.002	**0.967**	**0.990**	**0.993**	0.033	0.010	0.007
3	Condyle_M1	0.145	0.153	0.200	0.005	0.002	0.002	0.965	0.988	0.990	0.035	0.012	0.010
4	Ramus_Ht_Occlusal	**1.632**	**1.346**	0.714	0.075	0.027	0.027	0.954	0.980	0.962	0.046	0.020	0.038
5	Inter_P3_Br	0.504	0.359	0.656	0.058	0.032	**0.048**	0.886	0.910	0.926	0.114	0.090	0.074
6	Inter_M2_Br	0.466	0.360	0.544	0.062	0.030	0.042	0.868	0.915	0.923	0.132	0.085	0.077
7	Sym_Ht	0.534	0.420	0.360	0.074	0.031	0.040	0.862	0.927	0.888	0.138	0.073	0.112
8	Sym_Br	0.929	0.704	0.567	**0.081**	**0.043**	0.043	0.912	0.939	0.925	0.088	0.061	0.075
9	M2_Corp_Ht	0.576	0.305	0.371	0.046	0.020	0.033	0.920	0.934	0.912	0.080	0.066	0.088
10	M2_Corp_Br	1.034	0.567	0.536	0.075	0.032	0.040	0.927	0.943	0.926	0.073	0.057	0.074
11	P4_Br	0.321	0.623	0.452	0.064	0.043	0.034	0.799	0.932	0.925	0.201	0.068	0.075
12	M2_Br	0.273	0.435	0.282	0.053	0.033	0.035	0.806	0.923	0.876	0.194	0.077	0.124
13	PM_alveolar_Ln	0.536	0.438	0.242	0.068	0.038	0.035	0.873	0.914	0.854	0.127	0.086	0.146
14	Molar_alveolar_Ln	0.156	0.311	0.210	0.034	0.025	0.020	0.779	0.920	0.905	0.221	0.080	0.095
15	Canine_Ln	0.434	0.375	0.254	0.054	0.041	0.033	0.875	0.892	0.869	0.125	0.108	0.131
16	Bilat_Incisor	0.667	0.346	0.457	0.070	0.038	0.040	0.895	0.890	0.912	0.105	**0.110**	0.088
17	Ramus_Ht	0.590	0.507	0.235	0.076	0.035	0.039	0.872	0.930	0.836	0.128	0.070	**0.164**
18	Ramus_Br	0.344	0.366	0.290	0.077	0.036	0.036	0.776	0.901	0.877	**0.224**	0.099	0.123
19	M1_Corp_Ht	0.478	0.445	0.437	0.039	0.033	0.026	0.919	0.927	0.939	0.081	0.073	0.061
20	M1_Corp_Br	1.146	0.503	**0.738**	0.066	0.039	0.037	0.942	0.923	0.950	0.058	0.077	0.050

Abbreviations: *H.s.* = *Homo sapiens*; *P.t.* = *Pan troglodytes*; *G.g.* = *Gorilla gorilla*.
[a] See Table 2 for abbreviation of linear measurements.
[b] Multiplied by 10^2.
[c] Highest trait-wise evolvability, conditional evolvability, and integration values are bolded.

mean-standardized) and shape (scaled by geometric mean and mean-standardized) datasets are consistently high (between 0.81 and 0.97) and are always higher for the two African apes than for comparisons involving modern humans, although these differences are minimal for the form dataset (Table 5). It is possible that these high correlation coefficients may be a 'statistical artifact' reflecting the negative correlation between average trait value and trait variance mentioned previously (Rohlf et al., 1983). Nevertheless, the skull of gorillas is larger than those of the more similarly sized *H. sapiens* and *P. troglodytes* (SOM Tables S6 and S7). Thus, the higher correlation between the two African apes may not be attributed to their cranial size variation.

High correlations indicate that between-species differences are subtle. Bivariate plots help to highlight which traits are most divergent in each species with regard to evolvability. In the cranium, breadth of the midzygomatic arch (trait 1) and minimum thickness of the zygomatic root (trait 14) have proportionally higher e and c values in African apes than in *H. sapiens*, whereas the height of the midzygomatic arch (trait 2) and minimum thickness of the zygomatic root (trait 14) have consistently higher values in *P. troglodytes* than in *G. gorilla* in the form and shape datasets (Tables 6 and 7; Figs. 5–10).

In general, the corresponding correlation coefficients for e and c values for the mandible datasets (form and shape) are lower than

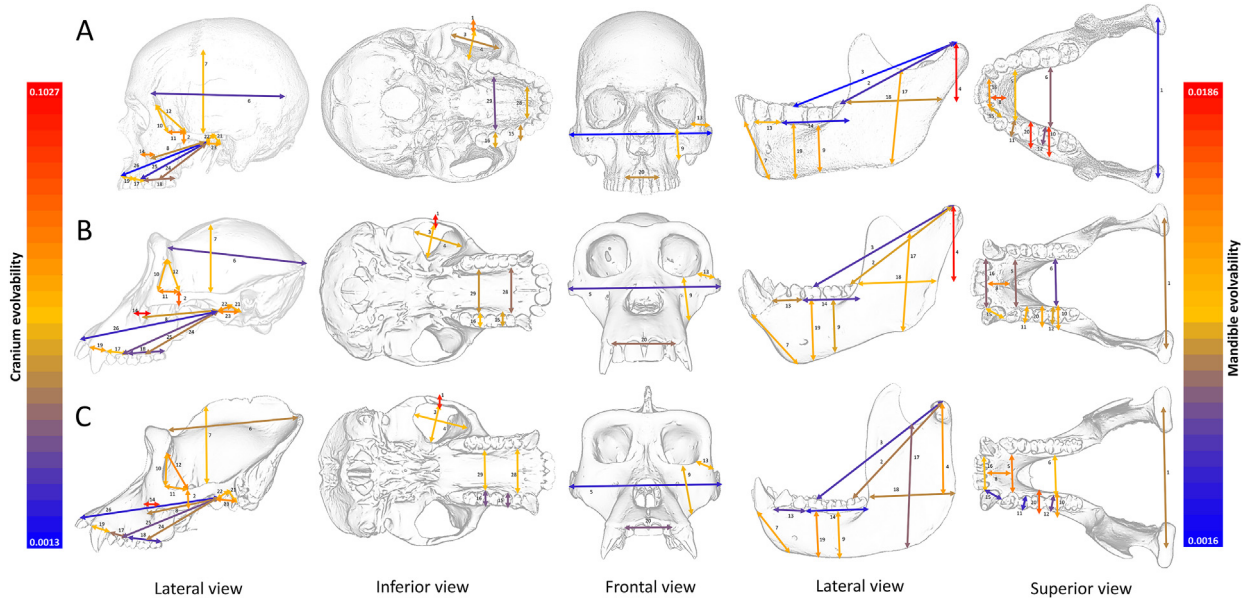

Figure 5. A visualization of evolvability (e) values in the form data. The A) human, B) chimpanzee and C) gorilla cranium and mandible are shown in lateral view. Red and blue colors show high and low e values in the cranium and mandible, respectively. Measurement of mechanical palate protrusion is not shown. Measurement error contributes to the proportionally high variation seen in absolutely small dimensions. Therefore, e values should only be directly compared for corresponding measurements across taxa or between measurements of similar scale. (For interpretation of the references to color in this figure legend, the reader is referred to the web version of this article.)

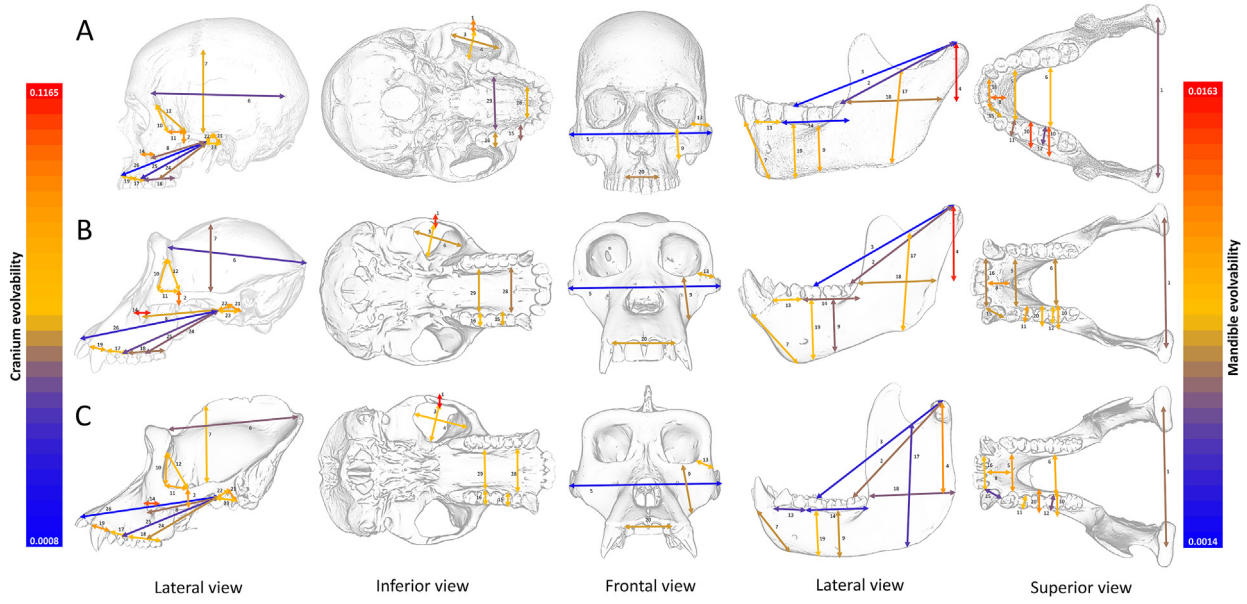

Figure 6. A visualization of evolvability (e) values in the shape data. The A) human, B) chimpanzee and C) gorilla cranium and mandible are shown in lateral view. Red and blue colors show high and low e values in the cranium and mandible, respectively. Measurement of mechanical palate protrusion is not shown. Measurement error contributes to the proportionally high variation seen in absolutely small dimensions. Therefore, conditional evolvability (c) values should only be directly compared for corresponding measurements across taxa or between measurements of similar scale. (For interpretation of the references to color in this figure legend, the reader is referred to the web version of this article.)

those in the cranial datasets. The *G. gorilla-P. troglodytes* comparisons are, in particular, only moderately correlated (0.44–0.58) with the exception of a higher c value (0.82) for mandibular shape (Table 5). The bivariate plots show correspondingly higher dispersion around the slope representing identical patterns between species, as well as the generally higher e and c values in *H. sapiens* (Tables 6 and 7; Figs. 5–8, 11, and 12).

The i statistic is informative about the extent to which a trait's covariance with the rest of the phenotype reduces its evolvability. For example, an i value of 0.90 indicates that 90% of that trait's variance is 'tied up' as covariance with the rest of the measured traits. Patterns of trait-by-trait i values are more highly correlated among species for cranial form (0.63–0.84) than for cranial shape (0.53–0.71) and are more similar between *G. gorilla* and *P. troglodytes* in both cases (Table 5). African apes have higher overall integration than *H. sapiens*, particularly with regard to maximum breadth of the temporal foramen (trait 4) and distance from the postglenoid process to the mandibular fossa in the form

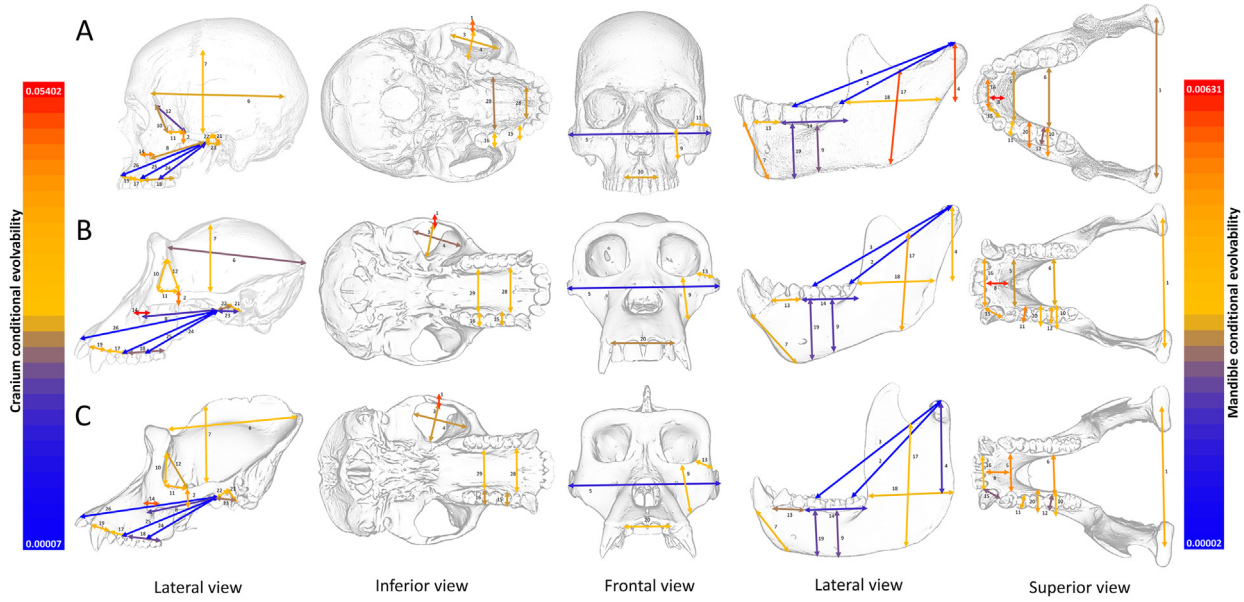

Figure 7. A visualization of conditional evolvability (c) values in the form data. The A) human, B) chimpanzee and C) gorilla cranium and mandible are shown in lateral view. Red and blue colors show high and low c values in the cranium and mandible, respectively. Measurement of mechanical palate protrusion is not shown. Measurement error contributes to the proportionally high variation seen in absolutely small dimensions. Therefore, c values should only be directly compared for corresponding measurements across taxa or between measurements of similar scale. (For interpretation of the references to color in this figure legend, the reader is referred to the web version of this article.)

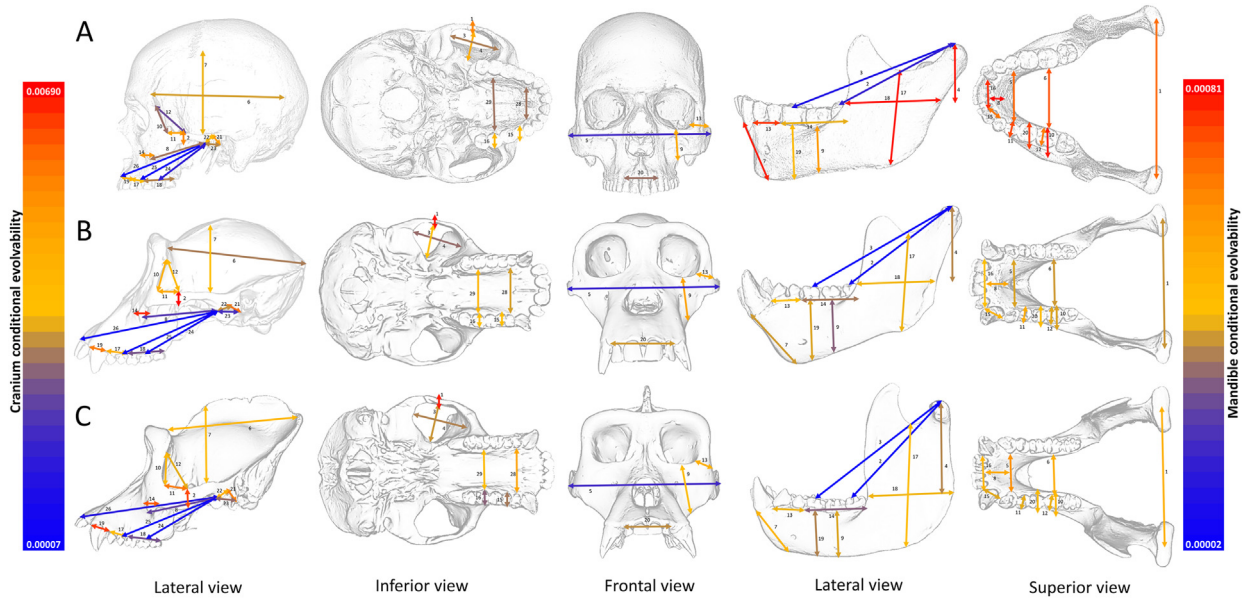

Figure 8. A visualization of conditional evolvability (c) values in the shape data. The A) human, B) chimpanzee and C) gorilla cranium and mandible are shown in lateral view. Red and blue colors show high and low c values in the cranium and mandible, respectively. Measurement of mechanical palate protrusion is not shown. Measurement error contributes to the proportionally high variation seen in absolutely small dimensions. Therefore, c values should only be directly compared for corresponding measurements across taxa or between measurements of similar scale. (For interpretation of the references to color in this figure legend, the reader is referred to the web version of this article.)

dataset (trait 21; Tables 6 and 7; Figs. 9, 10, 13, and 14). Moreover, the maxillary canine alveolar length (trait 19) and maxillary bilateral incisor alveolar length (trait 20) have particularly high i values in *P. troglodytes* compared to those in *G. gorilla* in the form dataset.

The mandibular form shows more similar patterns of integration (0.74–0.92) than the mandibular shape (0.62–0.72) for all species pairs, and the *G. gorilla* and *P. troglodytes* patterns are especially similar for the mandible form (0.92; Table 5). African apes show stronger integration than *H. sapiens* in the following traits in the form and shape datasets: mandibular bicondylar breadth (trait 1), ramus height above occlusal plane (trait 4), symphyseal height (trait 7), mandibular molar alveolar length (trait 14), and ramus breadth (trait 18; Tables 6 and 7; Figs. 11–14).

3.4. Magnitudes of integration

The V_{rel} and ICV statistics, which assess whether variance is spread along many dimensions (weak integration) or more concentrated into just a few axes (strong integration), indicates that humans exhibit weaker integration for cranial and mandibular

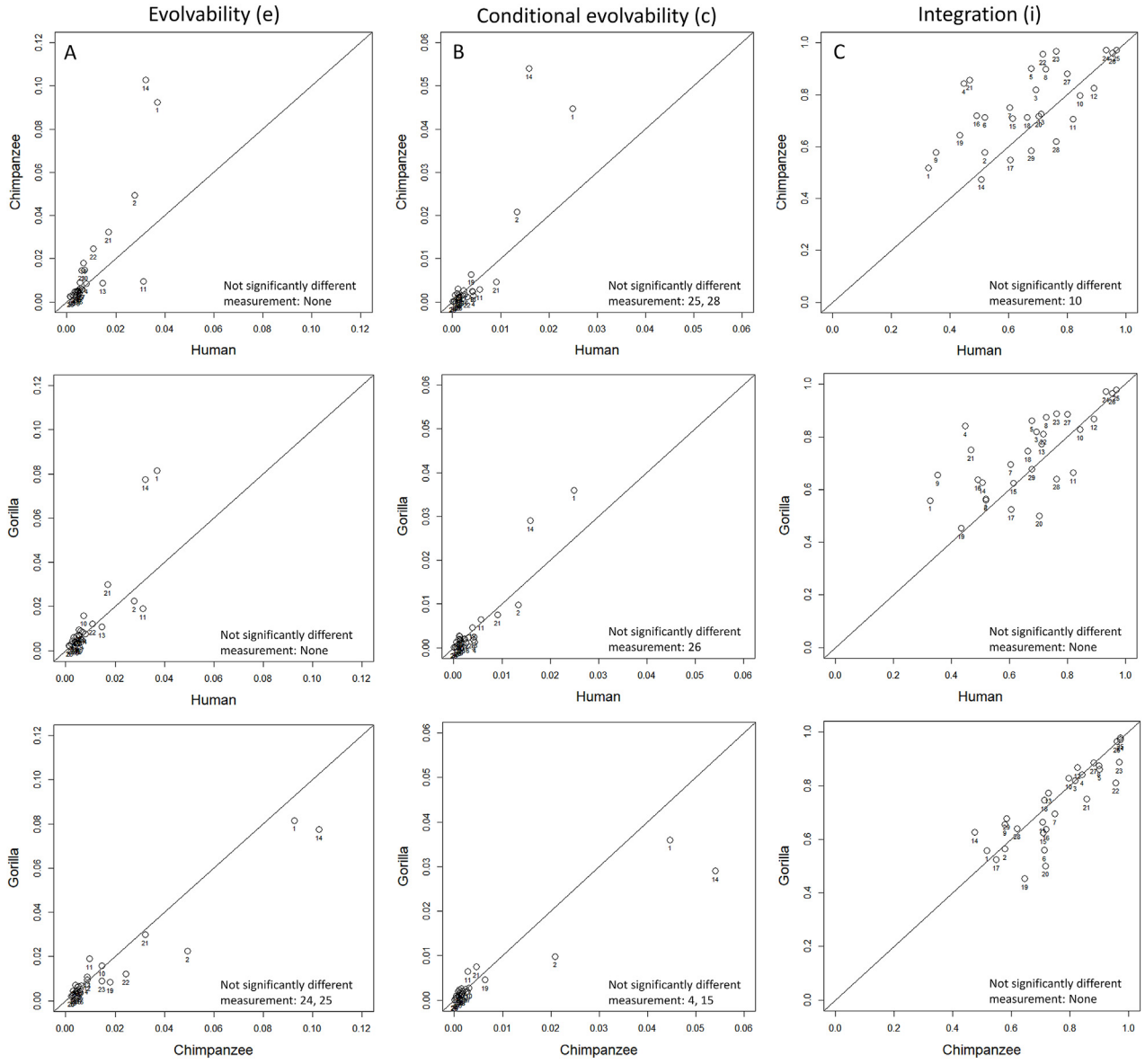

Figure 9. Scatterplots of evolvability (e; A), conditional evolvability (c; B), and integration (i; C) values in the cranium form. A line with a slope of 1 and y-intercept of 0 shows the expected relationship if the trait-wise evolutionary statistics are identical between taxa. Deviations from this line indicate differences in the pattern of integration among humans and chimpanzees (top), humans and gorillas (middle), and chimpanzees and gorillas (bottom).

form than the two African ape species, such as significantly lower ICV of humans than those of chimpanzees and gorillas (Table 8). The differences among species are smaller for the shape datasets, where humans have the highest V_{rel} value for cranial shape and gorillas having the highest V_{rel} value for mandibular shape. However, V_{rel} value was significantly different only between humans and gorillas in the mandibular shape data ($p < 0.05$).

4. Discussion

The current analysis is situated at the interface of evolutionary quantitative genetics and functional morphology. The results of this study provide an important comparative context for the pattern of functionally informative traits pertaining to the feeding biomechanics in African apes and modern humans. Trait integration captured by the G or P matrices is challenging to compare across species directly. We applied several analytical approaches to assess whether magnitudes and patterns of integration among biomechanically informative skull traits were congruent or divergent among *P. troglodytes*, *G. gorilla*, and *H. sapiens*.

We evaluated three hypotheses. The results indicate some support for Hypothesis 1, that patterns of integration among biomechanically informative traits are conserved across hominine species. In particular, comparisons of the P matrix and species-specific patterns of the trait-wise i statistic indicate conserved patterns of integration among biomechanically informative traits of the skull in the unscaled (form) dataset. The analyses of shape data provide weaker support for Hypothesis 1. The scaled cranial data (shape) show a greater divergence of species-specific PC 1's than in the form data, with nearly uncorrelated patterns between modern humans and chimpanzees. Likewise, while the trait-wise i values are strongly positively correlated among species for cranial shape, the correlation coefficients are lower than those in the cranial form dataset. The random skewers test still indicates a shared structure,

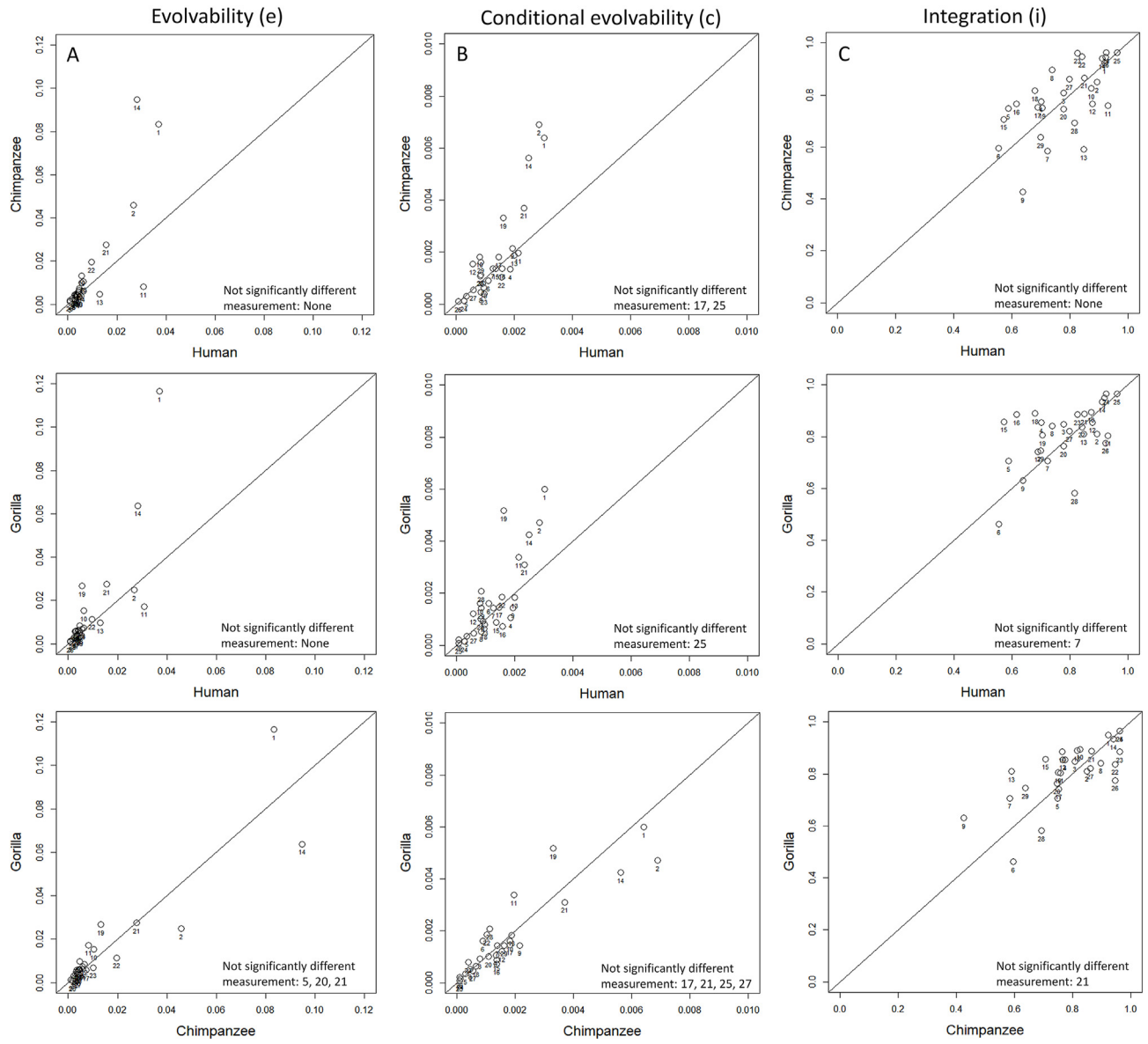

Figure 10. Scatterplots of evolvability (e; A), conditional evolvability (c; B), and integration (i; C) values in the cranium shape. A line with a slope of 1 and y-intercept of 0 shows the expected relationship if the trait-wise evolutionary statistics are identical between taxa. Deviations from this line indicate differences in the pattern of integration among humans and chimpanzees (top), humans and gorillas (middle), and chimpanzees and gorillas (bottom).

but less than that in the cranial form dataset. Analyses of the mandibular shape data also indicate some shared component of the integration pattern across species, but to a lesser extent than the form data.

Despite these generally conserved patterns of integration, however, the African apes are typically more similar in their integration patterns and are somewhat distinct from *H. sapiens*. These observations support Hypothesis 2 (i.e., more distinct patterns of integration in *H. sapiens* may be related to its evolutionary reorganization of skull morphology). The distinctiveness of the *H. sapiens* pattern is more apparent for the mandible than for the cranium based on the random skewers and species-specific PC 1 comparisons.

Homo sapiens had overall weaker integration as predicted, based on its less mechanically resistant and processed (e.g., agricultural) diet (Hypothesis 3). The one exception to this trend was the cranial shape, where humans had the highest integration magnitude, although the three values were similar. These results differ from the phylogenetically structured pattern of integration in face dimensions found in hominoids (Ackermann, 2002) and a weak to moderate phylogenetic signal across catarrhines (de Oliveira et al., 2009; but see Porto et al., 2009). Perhaps the covariance among biomechanically relevant traits of shape data does not strictly mirror the covariance among generalized, less functionally constrained skull traits.

4.1. Patterns of integration and biomechanical implications for unscaled data

The two African ape species had very similar patterns of integration for the cranial and mandibular form datasets (Tables 4 and 5; Fig. 3). The *H. sapiens* pattern of integration was more dissimilar, but all analyses still indicated a substantial shared structure. Traits reflecting differences in the size of the temporalis muscle and/or orientation of the masseter muscle and therefore

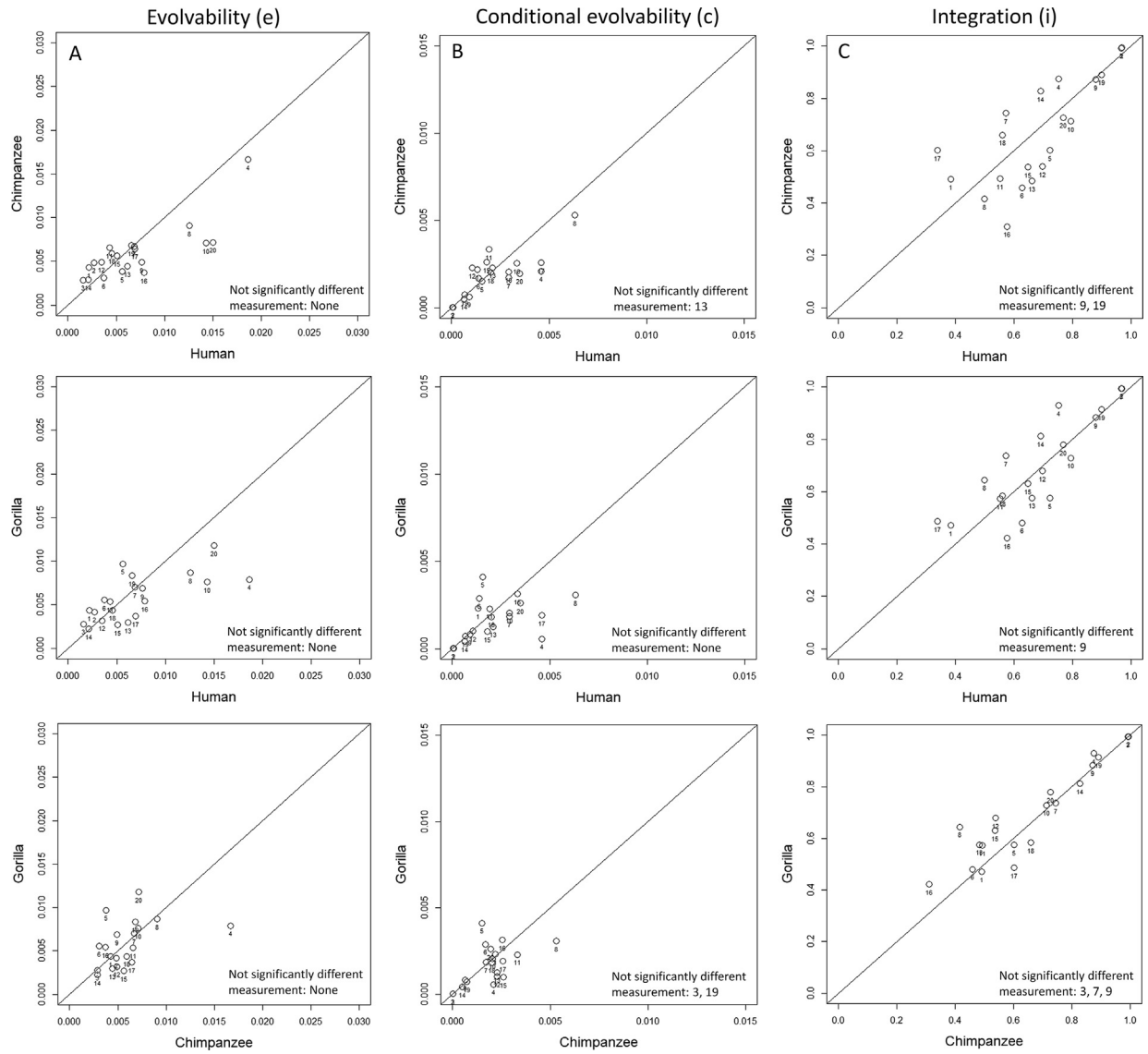

Figure 11. Scatterplots of evolvability (e; A), conditional evolvability (c; B), and integration (i; C) values in the mandible form. A line with a slope of 1 and y-intercept of 0 shows the expected relationship if the trait-wise evolutionary statistics are identical between taxa. Deviations from this line indicate differences in the pattern of integration among humans and chimpanzees (top), humans and gorillas (middle), and chimpanzees and gorillas (bottom).

affecting the magnitude of bite forces (bizygomatic breadth and maximum length and height of the temporalis muscle; traits 5, 6, and 7) load heavily on the PC 1 for the unscaled cranial measure in all the three species. Projection of the anterior maxilla (prosthion and the second premolar) from the articular eminence (traits 25 and 26) also loads strongly on the PC 1 and relates to the I^1 and P^4 load arms, which impact mechanical advantage during biting at those teeth. Moreover, the ramus height above occlusal plane (trait 4), bicondylar breadth (trait 1), and distance from the condyle to M_1 or M_3 (traits 2 and 3) load heavily on the PC 1 of the mandible form data in *H. sapiens*, *P. troglodytes*, and *G. gorilla*. These four traits are related to the triangle of support and affect the ability of the skull to prevent distraction of the condyle from the TMJ during molar bite force generation (Fig. 1; Greaves, 1978; Spencer, 1999). For instance, broader bicondylar breadth and higher ramus height above the occlusal plane reconfigure and incline the triangle of support, respectively, which in turn affects balancing side muscle force during molar bites. Thus, the current study suggests that integration in unscaled biomechanical traits across all the three hominine species facilitates coordinated changes to the jaw adductor muscle size and the triangle of support, both of which relate to bite force production. Nevertheless, caution is warranted because absolutely larger dimensions have higher loadings on the PC 1 axis for the unscaled data, which may result in more similar patterns of integration across the three taxa than for the shape (scaled) data.

4.2. Patterns of integration and biomechanical implications for shape (scaled) data

The greatest differences in integration pattern were between *H. sapiens* and *P. troglodytes* in cranial shape data and between *H. sapiens* and the two African apes in the mandible shape data. Temporalis length and height (traits 6 and 7) load heavily on the first dimension of cranial shape variation in humans and *G. gorilla* but less so in *P. troglodytes*. In contrast, the African ape species have high positive loadings for several traits that reflect facial projection anterior to the articular eminence (traits 8, 24, 25, and 26), whereas

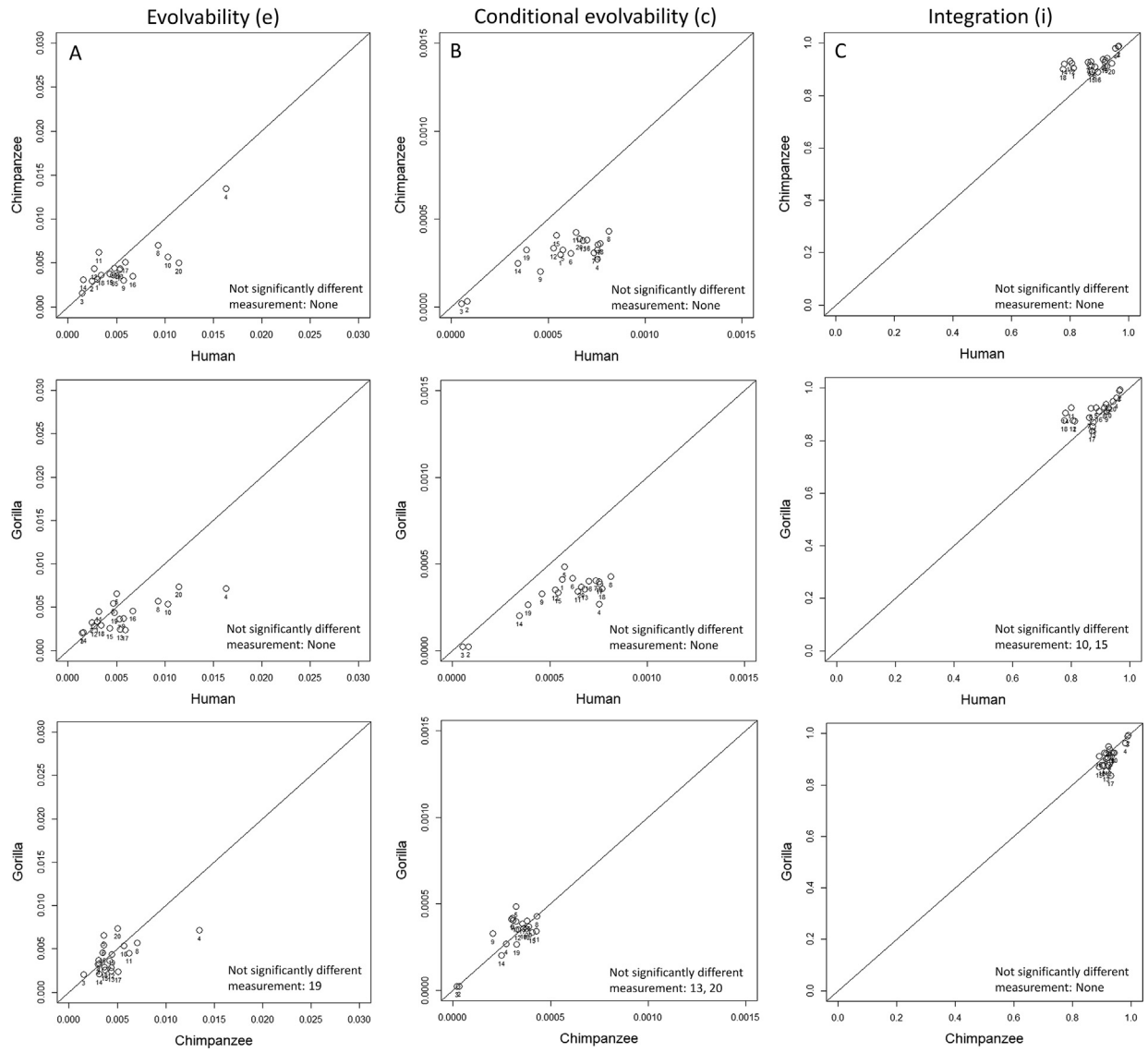

Figure 12. Scatterplots of evolvability (e; A), conditional evolvability (c; B), and integration (i; C) values in the mandible shape. A line with a slope of 1 and y-intercept of 0 shows the expected relationship if the trait-wise evolutionary statistics are identical between taxa. Deviations from this line indicate differences in the pattern of integration among humans and chimpanzees (top), humans and gorillas (middle), and chimpanzees and gorillas (bottom).

the same traits load negatively on the PC 1 in *H. sapiens*. The primary axis of shape variation in the mandible is also distinct in humans compared to chimpanzees and gorillas. Bicondylar breadth (trait 1) loads more heavily in *H. sapiens*, whereas condylar elevation above the occlusal plane (trait 4) loads more heavily in apes, which can be associated with location of muscle resultant force and properties of the triangle of support (Greaves, 1978; Spencer, 1999), suggesting different mechanisms in humans and African apes for maintaining bite force production using balancing side muscles and preventing working side condyle distraction. For example, increasing bicondylar breadth may alleviate the detrimental effect of a more parabolic dental arch (i.e., greater intercorpus breadth) in humans for bite force production. Moreover, increases in ramus height above the occlusal plane can incline the triangle of support and may allow a more anteriorly positioned or inclined muscle resultant force (i.e., longer muscle lever arm) with reduced risk of condyle distraction at the TMJ. The previous discussion of how the jaw adductor size, triangle of support, and mechanical advantage during biting influence bite force is also relevant here, given the overlap among key traits between the form and shape PC 1s. However, species differences in PC 1 loadings for cranial and mandibular shape mean that, for example, a relatively large temporalis in *H. sapiens* does not covary with increased mechanical advantage during biting on the anterior dentition for the shape dataset.

However, although the current study investigates biomechanically informative measurements, these dimensions are also affected by other nonfeeding factors. For example, temporalis attachment on the lateral vault wall and mechanical advantage during biting at the premolars and incisors are affected by neurocranial globularity and facial orthognathism, respectively. A retracted face decreases the relative length of the load arm (the distance between articular eminence and biting point) to lever arm, which results in increased mechanical advantage for both masseter and temporalis muscles. Facial retraction may result from developmental constraints in the skull architecture related to the influence of brain size and cranial base morphology on the vault and face (Lieberman, 2011; Neaux et al., 2018). In other

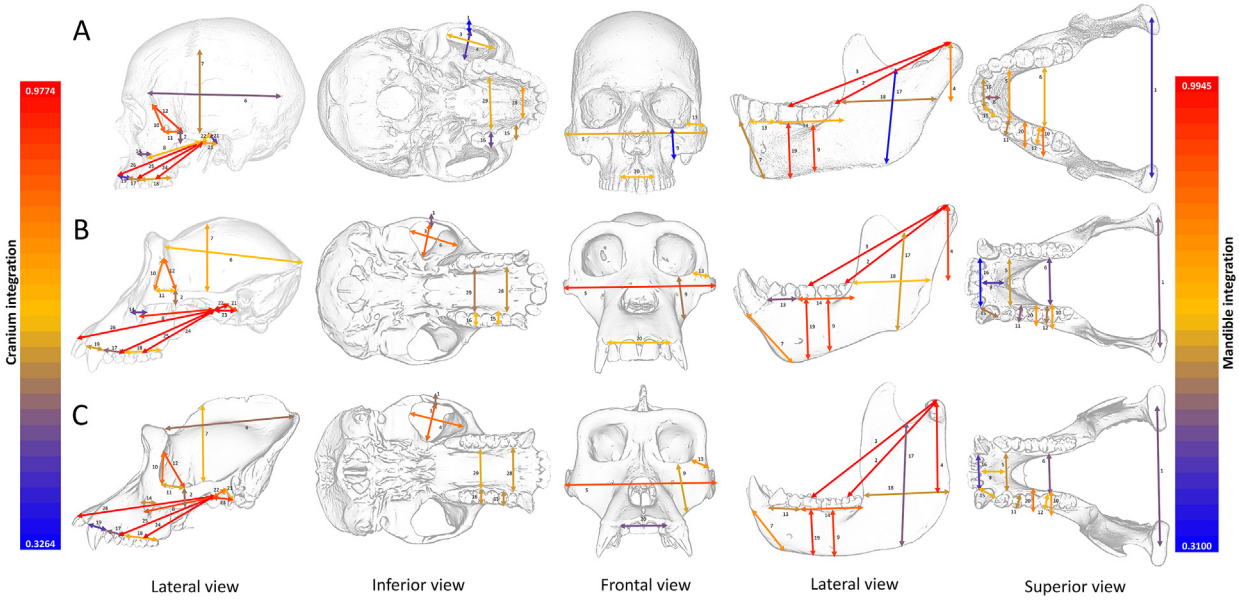

Figure 13. A visualization of integration (i) values in the form data. The A) human, B) chimpanzee and C) gorilla cranium and mandible are shown in lateral view. Red and blue colors show high and low i values in the cranium and mandible, respectively. Measurement of mechanical palate protrusion is not shown. (For interpretation of the references to color in this figure legend, the reader is referred to the web version of this article.)

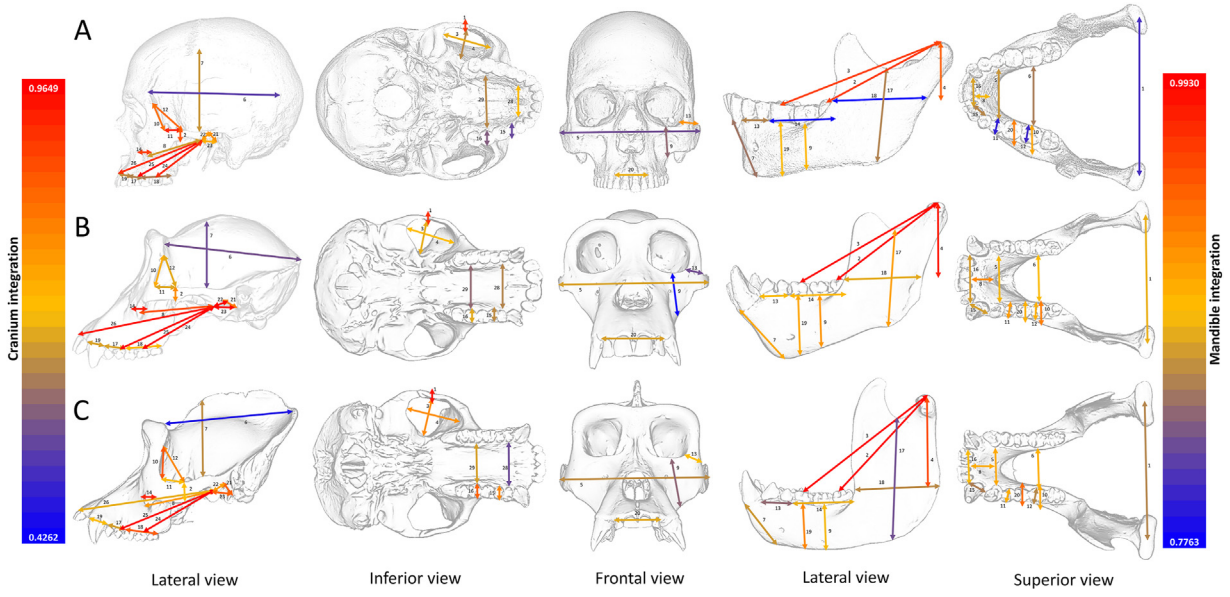

Figure 14. A visualization of integration (i) values in the shape data. The A) human, B) chimpanzee and C) gorilla cranium and mandible are shown in lateral view. Red and blue colors show high and low i values in the cranium and mandible, respectively. Measurement of mechanical palate protrusion is not shown. (For interpretation of the references to color in this figure legend, the reader is referred to the web version of this article.)

words, increased mechanical advantage in modern humans due to facial retraction may be a by-product of changes in brain size and associated neurocranial morphology. Thus, a globular cranial vault and retracted face characterize *H. sapiens*, and this may represent a shift in integration patterns associated with evolutionary changes to the mean shape of the skull from an ape-like ancestor to *H. sapiens* (Lieberman, 2011).

4.3. Trait-wise evolutionary statistics

Evolutionary statistics (sensu Hansen and Houle, 2008) were similarly patterned across all three taxa in the cranium but less in the mandible, whereas i values were more variable and not as strongly correlated across species. For example, most traits for jaw lever mechanics in the cranium (e.g., triangle of support) showed low e/c and high i values, which suggests a common 'constraint' shared across all the three taxa. The form data were more congruent than the shape data for evolutionary statistics as also seen in the results of other analyses discussed previously. Humans showed higher evolutionary potential in many traits (i.e., e and/or c) than the two African apes, although the differences are subtle in bivariate plots. This tendency was most pronounced in the mandibular shape data. These results correspond to previous studies that reported a high evolutionary rate in the hominin

Table 8
Relative eigenvalue variance with its standardized effect size (Z_{Vrel}) in parentheses and integration coefficient of variation values in the cranium and mandible.[a]

Skull region	Taxa	V_{rel}		ICV	
		Form	Shape[b]	Form	Shape[b]
Cranium	*H.s.*	0.427 (1.467[c])	0.422 (1.456)	2.093*,$	1.897$
	P.t.	0.489 (1.593)	0.330 (1.260)	2.556*,※	1.863※
	G.g.	0.580 (1.775)	0.294 (1.176)	2.458$,※	1.734$,※
Mandible	*H.s.*	0.233 (0.800)$	0.315 (1.008)	1.458*,$	1.604*,$
	P.t.	0.526 (1.448)	0.332 (1.045)	1.996*,※	1.595*,※
	G.g.	0.561 (1.518)$	0.515 (1.426)	2.065$,※	1.773$,※

Abbreviations: *H.s.* = *Homo sapiens*; *P.t.* = *Pan troglodytes*; *G.g.* = *Gorilla gorilla*; V_{rel} = relative eigenvalue variance; ICV = integration coefficient of variation.

[a] An asterisk (*) indicates statistically significant difference between *H.s.*—*P.t.* pair and *H.s.*—*G.g.* pair. A dollar sign ($) indicates statistically significant difference between *H.s.*—*P.t.* pair and *P.t.*—*G.g.* pair; A reference mark (※) indicates statistically significant difference between *H.s*—*G.g.* pair and *P.t*—*G.g.* pair. Statistically significant when $p < 0.05$.

[b] Shape data are the raw dimensions scaled by geometric mean of each individual.

[c] Z_{Vrel} was translated to a positive scale so that it cannot be zero (Conaway and Adams, 2022).

cranium/mandible using 'generic' morphological traits (e.g., Schroeder and von Cramon-Taubadel, 2017; Raia et al., 2018; von Cramon-Taubadel et al., 2021). For example, Raia et al. (2018) showed that hominins have an exceptionally rapid evolutionary rate in the mandibular shape compared to the other primate clades. Moreover, Schroeder and von Cramon-Taubadel (2017) reported that humans experienced strong directional selection on craniofacial morphology compared to other great apes. Our study provides additional empirical evidence of generally higher evolutionary potential in human skull morphology with biomechanically informative traits in relation to feeding.

4.4. Implications for studying microevolutionary and macroevolutionary processes in form/shape of feeding system

Previous studies reported generally similar structures of P matrices (i.e., patterns of integration) among hominoids, including *Homo*, *Pan*, and *Gorilla*, for overall skull morphology even though different data types (coordinates vs. linear distances) and analytic methods were applied (Ackermann, 2002; de Oliveira et al., 2009; Marroig et al., 2009; Porto et al., 2009; Singh et al., 2012; Neaux, 2017). The present study adds new empirical evidence that craniometric measurements associated with the feeding system also have similar, but nonidentical, patterns of integration among *H. sapiens*, *P. troglodytes*, and *G. gorilla* but more so for unscaled than for size-scaled dimensions. Patterns of evolutionary statistics were also similar across all the three taxa. It follows that the covariance structure of biomechanically informative craniometric measurements may also be under stabilizing selection among humans and the African apes. Thus, the same primary pattern of variation is maintained across all the three species with only subtle variations observed, and it can be inferred that *H. sapiens*, *P. troglodytes*, and *G. gorilla* share similar constraints for morphological variation in feeding system for applying bite force and resisting reaction forces.

Empirical evidence suggests that morphological integration affects not just microevolution but also macroevolution, including divergence between taxa (e.g., the superfamily Hominoidea, family Hominidae, or subfamily Homininae; Schluter, 1996; Arnold et al., 2001; Marroig and Cheverud, 2005; Marroig et al., 2009; Baab, 2018). Evaluating the influence of population-wide patterns of trait variance and covariance on macroevolution requires an assumption of consistent integration patterns (i.e., covariance structure) along the branches to ancestral nodes and/or terminal taxa in a phylogenetic tree (Schluter, 1996; Arnold et al., 2001; Marroig and Cheverud, 2005; Marroig et al., 2009). The results of the present study suggest that it is reasonable to use *H. sapiens*, *P. troglodytes*, and *G. gorilla* as proxies for extinct hominin taxa (see also Ackermann, 2002) but with more caution in the case of mandible shape. Although these results could be modified if a different human population or subspecies of African apes were analyzed, we expect the impact of sampling to be minimal, given the generally conserved pattern of functional integration we documented here.

5. Conclusions

In the present study, it was shown that integration patterns in craniofacial measurements reflecting feeding biomechanics were generally similar, but not identical, among *H. sapiens*, *P. troglodytes*, and *G. gorilla*. Traits associated with size and/or shape of the temporalis and masseter muscle and with the triangle of support were the most influential on the primary axis of variation in morphospace (e.g., p_{max}). After mean standardization, evolutionary statistics were also similarly patterned across the three taxa, while humans showed higher evolutionary potential in many traits. The relatively consistent integration pattern and its evolutionary consequences may suggest opportunities for investigating macroevolutionary processes in the feeding system of extinct hominins for which population parameters are not directly measurable by using the extant hominines as proxies. Although linear measurements in the present study are biomechanically informative, there may be no one-to-one relationship between the linear measurements and the ability to generate muscle force and/or to resist loading from feeding forces (reviewed in Ross and Iriarte-Diaz, 2019). Thus, certain differences in patterns of functional morphological integration may not be detected in the present study. In future studies, it may be helpful to apply more diverse biomechanical variables from experimental data, such as the variations in muscle activation patterns, to overcome the limitation of this study.

Declaration of competing interest

None.

Acknowledgments

We are grateful to Claire Terhune, Jason Massey, and Kieran McNulty for providing three dimentional surface scans. We thank Brenda J. Baker at the Arizona State University, Yohannes Haile-Selassie at the Cleveland Museum of Natural History, Lawrence Heaney at the Field Museum of Natural History, Darrin Lunde at the Smithsonian Museum of Natural History, Mark Omura at the Museum of Comparative Zoology at the Harvard University, and staff at the American Museum of Natural History for granting access to skeletal materials for data collection. We thank Jenni Lord and Monica Castro for methodological assistance during the early stages of data collection. This material is based upon work supported by the National Science Foundation under grant number BCS-2019669.

Supplementary Online Material

Supplementary online material to this article can be found online at https://doi.org/10.1016/j.jhevol.2023.103401.

References

Ackermann, R.R., 2002. Patterns of covariation in the hominoid craniofacial skeleton: Implications for paleoanthropological models. J. Hum. Evol. 43, 167–187.

Ackermann, R.R., Cheverud, J.M., 2004. Detecting genetic drift versus selection in human evolution. Proc. Natl. Acad. Sci. USA 101, 17946–17951.
Arnold, S.J., Pfrender, M.E., Jones, A.G., 2001. The adaptive landscape as a conceptual bridge between micro-and macroevolution. Genetica 112–113, 9–32.
Arnold, S.J., Bürger, R., Hohenlohe, P.A., Ajie, B.C., Jones, A.G., 2008. Understanding the evolution and stability of the G-matrix. Evolution 62, 2451–2461.
Baab, K.L., 2018. Evolvability and craniofacial diversification in genus *Homo*. Evolution 72, 2781–2791.
Baken, E.K., Collyer, M.L., Kaliontzopoulou, A., Adams, D.C., 2021. geomorph v4. 0 and gmShiny: Enhanced analytics and a new graphical interface for a comprehensive morphometric experience. Methods Ecol. Evol. 12, 2355–2363.
Bastir, M., Rosas, A., Sheets, H.D., 2005. The morphological integration of the hominoid skull: A partial least squares and PC analysis with implications for European Middle Pleistocene mandibular variation. In: Slice, D.E. (Ed.), Modern Morphometrics in Physical Anthropology. Springer, Boston, pp. 265–284.
Bookstein, F.L., 1989. Principal warps: Thin-plate splines and the decomposition of deformations. IEEE Trans. Pattern Anal. Mach. Intell. 2, 567–585.
Cheverud, J.M., 1982. Phenotypic, genetic, and environmental morphological integration in the cranium. Evolution 36, 499–516.
Cheverud, J.M., 1996. Developmental integration and the evolution of pleiotropy. Am. Zool. 36, 44–50.
Cheverud, J.M., Rutledge, J.J., Atchley, W.R., 1983. Quantitative genetics of development: Genetic correlations among age-specific trait values and the evolution of ontogeny. Evolution 37, 895–905.
Cheverud, J.M., Marroig, G., 2007. Comparing covariance matrices: Random skewers method compared to the common principal components model. Genet. Mol. Biol. 30, 461–469.
Conaway, M.A., Adams, D.C., 2022. An effect size for comparing the strength of morphological integration across studies. Evolution 76, 2244–2259.
de Oliveira, F.B., Porto, A., Marroig, G., 2009. Covariance structure in the skull of Catarrhini: A case of pattern stasis and magnitude evolution. J. Hum. Evol. 56, 417–430.
Dumont, E.R., Herrel, A., 2003. The effects of gape angle and bite point on bite force in bats. J. Exp. Biol. 206, 2117–2123.
Fedorov, A., Beichel, R., Kalpathy-Cramer, J., Finet, J., Fillion-Robin, J.C., Pujol, S., Bauer, C., Jennings, D., Fennessy, F., Sonka, M., Buatti, J., Aylward, S., Miller, J.V., Pieper, S., Kikinis, R., 2012. 3D Slicer as an image computing platform for the quantitative imaging network. Magn. Reson. Imaging 30, 1323–1341.
Flury, B., 1988. Common Principal Components & Related Multivariate Models. John Wiley & Sons, Inc, New York.
Galland, M., van Gerven, D.P., von Cramon-Taubadel, N., Pinhasi, R., 2016. 11,000 years of craniofacial and mandibular variation in Lower Nubia. Sci. Rep. 6, 31040.
Gómez-Robles, A., Polly, P.D., 2012. Morphological integration in the hominin dentition: Evolutionary, developmental, and functional factors. Evolution 66, 1024–1043.
Goswami, A., Polly, P.D., 2010. The influence of modularity on cranial morphological disparity in Carnivora and Primates (Mammalia). PLoS One 5, e9517.
Goswami, A., Watanabe, A., Felice, R.N., Bardua, C., Fabre, A.C., Polly, P.D., 2019. High-density morphometric analysis of shape and integration: The good, the bad, and the not-really-a-problem. ICB 59, 669–683.
Grabowski, M.W., Polk, J.D., Roseman, C.C., 2011. Divergent patterns of integration and reduced constraint in the human hip and the origins of bipedalism. Evolution 65, 1336–1356.
Greaves, W.S., 1978. The jaw lever system in ungulates: A new model. J. Zool. 184, 271–285.
Gunz, P., Mitteroecker, P., Neubauer, S., Weber, G.W., Bookstein, F.L., 2009. Principles for the virtual reconstruction of hominin crania. J. Hum. Evol. 57, 48–62.
Hakem, A.A., 1981. The civilization of Napata and Meroe. In: Mokhtar, G. (Ed.), General History of Africa II: Ancient Civilizations of Africa. University of California Press, Berkeley, pp. 198–325.
Hansen, T.F., Houle, D., 2008. Measuring and comparing evolvability and constraint in multivariate characters. J. Evol. Biol. 21, 1201–1219.
Herring, S.W., Herring, S.E., 1974. The superficial masseter and gape in mammals. Am. Nat. 108, 561–576.
Hylander, W.L., 1988. Implications of in vivo experiments for interpreting the functional significance of "robust" australopithecine jaws. In: Grine, F.E. (Ed.), Evolutionary History of the "Robust" Australopithecines. Aldine Transaction, New Brunswick, pp. 55–83.
Hylander, W.L., Ravosa, M.J., Ross, C.F., Johnson, K.R., 1998. Mandibular corpus strain in primates: Further evidence for a functional link between symphyseal fusion and jaw-adductor muscle force. Am. J. Phys. Anthropol. 107, 257–271.
Jungers, W.L., Falsetti, A.B., Wall, C.E., 1995. Shape, relative size, and size-adjustments in morphometrics. Am. J. Phys. Anthropol. 38, 137–161.
Klingenberg, C.P., 2014. Studying morphological integration and modularity at multiple levels: Concepts and analysis. Philos. Trans. R. Soc. B 369, 20130249.
Lande, R., 1979. Quantitative genetic analysis of multivariate evolution, applied to brain: Body size allometry. Evolution 33, 402–416.
Lester, J.D., Vigilant, L., Gratton, P., McCarthy, M.S., Barratt, C.D., Dieguez, P., Agbor, A., Álvarez-Varona, P., Angedakin, S., Ayimisin, E.A., Bailey, E., Bessone, M., Brazzola, G., Chancellor, R., Cohen, H., Danquah, E., Deschner, T., Egbe, V.E., Eno-Nku, M., Goedmakers, A., Granjon, A., Head, J., Hedwig, D., Hernandez-Aguilar, R.A., Jeffery, K.J., Jones, S., Junker, J., Kadam, P., Kaiser, M., Kalan, A.K., Kehoe, L., Kienast, I., Langergraber, K.E., Lapuente, J., Laudisoit, A., Lee, K., Marrocoli, S., Mihindou, V., Morgan, D., Muhanguzi, G., Neil, E., Nicholl, S., Orbell, C., Ormsby, L.J., Pacheco, L., Piel, A., Robbins, M.M., Rundus, A., Sanz, C., Sciaky, L., Siaka, A.M., Städele, V., Stewart, F., Tagg, N., Ton, E., Schijndel, J.V., Vyalengerera, M.K., Wessling, E.G., Willie, J., Wittig, R.M., Yuh, Y.G., Yurkiw, K., Zuberbuehler, K., Boesch, C., Kühl, H.S., Arandjelovic, M., 2021. Recent genetic connectivity and clinal variation in chimpanzees. Commun. Biol. 4, 283.
Lieberman, D., 2011. The Evolution of the Human Head. Harvard University Press, Cambridge.
Lockwood, C.A., 2007. Adaptation and functional integration in primate phylogenetics. J. Hum. Evol. 52, 490–503.
Makedonska, J., Wright, B.W., Strait, D.S., 2012. The effect of dietary adaption on cranial morphological integration in capuchins (order Primates, genus *Cebus*). PLoS One 7, e40398.
Marroig, G., Cheverud, J.M., 2004. Did natural selection or genetic drift produce the cranial diversification of neotropical monkeys? Am. Nat. 163, 417–428.
Marroig, G., Cheverud, J.M., 2005. Size as a line of least evolutionary resistance: Diet and adaptive morphological radiation in New World monkeys. Evolution 59, 1128–1142.
Marroig, G., Shirai, L.T., Porto, A., de Oliveira, F.B., De Conto, V., 2009. The evolution of modularity in the mammalian skull II: Evolutionary consequences. Evol. Biol. 36, 136–148.
Martínez-Abadías, N., Esparza, M., Sjøvold, T., González-José, R., Santos, M., Hernández, M., Klingenberg, C.P., 2012. Pervasive genetic integration directs the evolution of human skull shape. Evolution 66, 1010–1023.
Melo, D., Garcia, G., Hubbe, A., Assis, A.P., Marroig, G., 2015. EvolQG-An R package for evolutionary quantitative genetics. F1000Res. 4.
Mitteroecker, P., Bookstein, F., 2008. The evolutionary role of modularity and integration in the hominoid cranium. Evolution 62, 943–958.
Neaux, D., 2017. Morphological integration of the cranium in *Homo*, *Pan*, and *Hylobates* and the evolution of hominoid facial structures. Am. J. Phys. Anthropol. 162, 732–746.
Neaux, D., Sansalone, G., Ledogar, J.A., Ledogar, S.H., Luk, T.H., Wroe, S., 2018. Basicranium and face: Assessing the impact of morphological integration on primate evolution. J. Hum. Evol. 118, 43–55.
Noback, M.L., Harvati, K., 2015. Covariation in the human masticatory apparatus. Anat. Rec. 298, 64–84.
Olson, E.C., Miller, R.L., 1958. Morphological Integration. University of Chicago Press, Chicago.
Paschetta, C., De Azevedo, S., González, M., Quinto-Sánchez, M., Cintas, C., Varela, H., Gómez-Valdés, J., Sánchez-Mejorada, G., González-José, R., 2016. Shifts in subsistence type and its impact on the human skull's morphological integration. Am. J. Hum. Biol. 28, 118–128.
Pavlicev, M., Cheverud, J.M., Wagner, G.P., 2009. Measuring morphological integration using eigenvalue variance. Evol. Biol. 36, 157–170.
Pepler, P.T., Uys, D.W., Nel, D.G., 2016. A comparison of some methods for the selection of a common eigenvector model for the covariance matrices of two groups. Commun. Stat. Simulat. 45, 2917–2936.
Phillips, P.C., Arnold, S.J., 1999. Hierarchical comparison of genetic variance-covariance matrices. I. Using the Flury hierarchy. Evolution 53, 1506–1515.
Polly, P.D., 2020. Functional tradeoffs carry phenotypes across the valley of the shadow of death. Integr. Comp. Biol. 60, 1268–1282.
Porto, A., de Oliveira, F.B., Shirai, L.T., De Conto, V., Marroig, G., 2009. The evolution of modularity in the mammalian skull I: Morphological integration patterns and magnitudes. Evol. Biol. 36, 118–135.
Profico, A., Piras, P., Buzi, C., Di Vincenzo, F., Lattarini, F., Melchionna, M., Veneziano, A., Raia, P., Manzi, G., 2017. The evolution of cranial base and face in Cercopithecoidea and Hominoidea: Modularity and morphological integration. Am. J. Primatol. 79, e22721.
Prado-Martinez, J., Sudmant, P.H., Kidd, J.M., Li, H., Kelley, J.L., Lorente-Galdos, B., Veeramah, K.R., Woerner, A.E., O'Connor, T.D., Santpere, G., Cagan, A., Theunert, C., Casals, F., Laayouni, H., Munch, K., Hobolth, A., Halager, A.E., Malig, M., Hernandez-Rodriguez, J., Hernando-Herraez, I., Prüfer, K., Pybus, M., Johnstone, L., Lachmann, M., Alkan, C., Twigg, D., Petit, N., Baker, C., Hormozdiari, F., Fernandez-Callejo, M., Dabad, M., Wilson, M.L., Stevison, L., Camprubí, C., Carvalho, T., Ruiz-Herrera, A., Vives, L., Mele, M., Abello, T., Kondova, I., Bontrop, R.E., Pusey, A., Lankester, F., Kiyang, J.A., Bergl, R.A., Lonsdorf, E., Myers, S., Ventura, M., Gagneux, P., Comas, D., Siegismund, H., Blanc, J., Agueda-Calpena, L., Gut, M., Fulton, L., Tishkoff, S.A., Mullikin, J.C., Wilson, R.K., Gut, I.G., Gonder, M.K., Ryder, O.A., Hahn, B.H., Navarro, A., Akey, J.M., Bertranpetit, J., Reich, D., Mailund, T., Schierup, M.H., Hvilsom, C., Andrés, A.M., Wall, J.D., Bustamante, C.D., Hammer, M.F., Eichler, E.E., Marques-Bonet, T., 2013. Great ape genetic diversity and population history. Nature 499, 471–475.
R Core Team, 2021. R: A language and environment for statistical computing. R Foundation for Statistical computing, Vienna, Austria. URL. http://www.R-project.org/.
Raia, P., Boggioni, M., Carotenuto, F., Castiglione, S., Di Febbraro, M., Di Vincenzo, F., Melchionna, M., Mondanaro, A., Papini, A., Profico, A., Serio, C., Veneziano, A., Vero, V.A., Rook, L., Meloro, C., Manzi, G., 2018. Unexpectedly rapid evolution of mandibular shape in hominins. Sci. Rep. 8, 7340.
Ravosa, M.J., 1998. Cranial allometry and geographic variation in slow lorises (*Nycticebus*). Am. J. Primatol. 45, 225–243.
Roff, D.A., 1995. The estimation of genetic correlations from phenotypic correlations: A test of Cheverud's conjecture. Heredity 74, 481–490.
Rohlf, F.J., 2017. The method of random skewers. Evol. Biol. 44, 542–550.

Rohlf, F.J., Gilmartin, A.J., Hart, G., 1983. The Kluge-Kerfoot phenomenon–a statistical artifact. Evolution 37, 180–202.
Rolian, C., 2009. Integration and evolvability in primate hands and feet. Evol. Biol. 36, 100–117.
Ross, C.F., Iriarte-Diaz, J., 2019. Evolution, constraint, and optimality in primate feeding systems. In: Bels, V., Whishaw, I.Q. (Eds.), Feeding in Vertebrates. Springer, Cham, pp. 787–829.
Schluter, D., 1996. Adaptive radiation along genetic lines of least resistance. Evolution 50, 1766–1774.
Schroeder, L., Roseman, C.C., Cheverud, J.M., Ackermann, R.R., 2014. Characterizing the evolutionary path(s) to early *Homo*. PLoS One 9, e114307.
Schroeder, L., von Cramon-Taubadel, N., 2017. The evolution of hominoid cranial diversity: A quantitative genetic approach. Evolution 71, 2634–2649.
Shirai, L.T., Marroig, G., 2010. Skull modularity in neotropical marsupials and monkeys: size variation and evolutionary constraint and flexibility. J. Exp. Zool. B. 314, 663–683.
Singh, N., Harvati, K., Hublin, J.J., Klingenberg, C.P., 2012. Morphological evolution through integration: A quantitative study of cranial integration in *Homo, Pan, Gorilla* and *Pongo*. J. Hum. Evol. 62, 155–164.
Skelton, R.R., McHenry, H.M., 1992. Evolutionary relationships among early hominids. J. Hum. Evol. 23, 309–349.
Sokal, R.R., Rohlf, F.J., 2001. Biometry: The Principles of Statistics in Biological Research, 3rd ed. W. H. Freeman, New York.
Spencer, M.A., 1999. Constraints on masticatory system evolution in anthropoid primates. Am. J. Phys. Anthropol. 108, 483–506.
Steppan, S.J., Phillips, P.C., Houle, D., 2002. Comparative quantitative genetics: Evolution of the G matrix. Trends Ecol. Evol. 17, 320–327.
Strait, D.S., 2001. Integration, phylogeny, and the hominid cranial base. Am. J. Phys. Anthropol. 114, 273–297.
Strait, D.S., Constantino, P., Lucas, P.W., Richmond, B.G., Spencer, M.A., Dechow, P.C., Ross, C.F., Grosse, I.R., Wright, B.W., Wood, B.A., Weber, G.W., Wang, Q., Byron, C., Slice, D.E., Chalk, J., Smith, A.L., Wood, S., Berthaume, M., Benazzi, S., Dzialo, C., Tamvada, K., Ledogar, J.A., 2013. Viewpoints: Diet and dietary adaptations in early hominins: The hard food perspective. Am. J. Phys. Anthropol. 151, 339–355.
Vinyard, C.J., Taylor, A.B., Teaford, M.F., Glander, K.E., Ravosa, M.J., Rossie, J.B., Ryan, T.M., Williams, S.H., 2011. Are we looking for loads in all the right places? New research directions for studying the masticatory apparatus of New World monkeys. Anat. Rec. 294, 2140–2157.
von Cramon-Taubadel, N., Frazier, B.C., Lahr, M.M., 2007. The problem of assessing landmark error in geometric morphometrics: Theory, methods, and modifications. Am. J. Phys. Anthropol. 134, 24–35.
von Cramon-Taubadel, N., Scott, J.E., Robinson, C.A., Schroeder, L., 2021. The evolution of the human chin: A quantitative genetic analysis of hominoid craniomandibular form. Am. J. Phys. Anthropol. 174, 109–110.
White, T.D., Folkens, P.A., 2000. Human Osteology. Academic Press, New York.
Young, N.M., Wagner, G.P., Hallgrímsson, B., 2010. Development and the evolvability of human limbs. Proc. Natl. Acad. Sci. USA 107, 3400–3405.
Zelditch, M.L., Swiderski, D.L., Sheets, H.D., 2012. Geometric Morphometrics for Biologists: A Primer. Academic Press, New York.